"Hitting Two Birds with One Stone" Design of Intestinal Integrin-Targeting and Redox Homeostasis-Regulating Oral Nanotherapy for Ulcerative Colitis

Long Huang[1], Wei Hu[2], Long Qun Huang[1], Qin Xuan Zhou[2], Zheng Yang Song[2], Heng Yu Tao[2], Bing Xu[3], Can Yang Zhang[2,*], Yi Wang[1,*], Xin-Hui Xing[2,3,4,*].

1. Institute of Biochemical Engineering, Department of Chemical Engineering, Tsinghua University, Beijing 100084, China.

2. Institute of Biopharmaceutical and Health Engineering, Shenzhen International Graduate School, Tsinghua University, Shenzhen 518055, China.

3. Institute of Biomedical Health Technology and Engineering, Shenzhen Bay Laboratory, Shenzhen 518118, China.

4. Center for Synthetic and Systems Biology, Tsinghua University, Beijing 100084, China

[†]Corresponding author: Xinhui Xing;

Tel: 86-10-62794771, E-mail: xhxing@tsinghua.edu.cn;

[†]Corresponding author: Yi Wang;

Tel: 86-10-62773004, E-mail: wangyi671@mail.tsinghua.edu.cn;

[†]Corresponding author: Canyang Zhang;

E-mail: zhang.cy@sz.tsinghua.edu.cn;

Long Huang, E-mail: huanglon22@mails.tsinghua.edu.cn;

Abstract

Designing highly efficient oral nanotherapies with specific inflamed site-targeting function in the gastrointestinal (GI) tract for ulcerative colitis (UC) management remains a significant challenge. The straightforward and adaptable modular multifunctional nanotherapies are poised to drive breakthroughs and encourage broad application in both academic research and clinical practice. In this study, we focused on exploring a specific targeting modular and functional oral nanotherapy, serving as "one stone", for the directed localization of inflammation and the regulation of redox homeostasis, thereby achieving "two birds" effects for UC treatment. The nanotherapy (so-called OPNs@LMWH) with core-shell structure composed of oxidation-sensitive ε-polylysine nanoparticles (OPNs) in the core and low molecular weight heparin (LMWH) in the shell present active specific targeting effect and therapeutical effect simultaneously. We qualitatively and quantificationally confirmed that OPNs@LMWH possessed high integrin αM-mediated immune cellular uptake efficiency and preferentially accumulated in the inflamed lesions. Compared with naked OPNs, OPNs@LMWH formulation exhibited enhanced intracellular reactive oxygen species (ROS) scavenging and anti-inflammatory features. Upon oral administration in mice subjected to dextran sulfate sodium (DSS)-induced colitis, OPNs@LMWH exhibited a robust capacity for resilience. It effectively ameliorated oxidative stress and curtailed the activation of inflammation-associated signaling pathways, while simultaneously bolstering the protective mechanisms of the colonic epithelium. Overall, these findings underscore the compelling dual functionalities of OPNs@LMWH, which enable effective oral delivery to inflammation sites, thereby facilitating precise UC management.

Introduction

The global incidence and prevalence of ulcerative colitis (UC) which is a chronic remitting-relapsing inflammatory disorder of the large intestine, have been on the rapid rise worldwide, yet the disease remains incurable with a multifaceted pathophysiology[1-3]. European Crohn's and Colitis Organization (ECCO) and American Gastroenterological Association (AGA) recommend the patients for following a step-up approach to get the desired remission by chemical drugs or monoclonal antibodies, due to no known cure for UC in clinic[4-6]. However, the frequent and long-term use of conventional small-molecule therapeutics or biologics-based immunosuppressive drugs can lead to severe complications, such as opportunistic infections, malignancies, autoimmunity, and liver toxicity[7-9]. Herein, it is of great significance to develop effective therapeutics and treatment strategies for UC management. Inspired by the evidence-based understanding of inflammatory signaling and drug delivery methods, efficient UC therapy based on active component discovery and precise delivery could be rationally designed and developed[10].

In prior research, the precision of drug delivery has been identified as a significant challenge[11,12]. Precise delivery's success is fundamentally dependent on the judicious choice of targeting strategies. A variety of strategies have been devised to target intestinal inflammation sites, utilizing microbial enzyme degradation, pH values, and the phenomenon of mucosal charge reversal at the inflamed locations[13-17]. However, the complex and ever-changing environment of gastrointestinal diseases significantly undermines their reliability and precision for UC treatment outcomes [18]. Given the propensity of immune cells to

accumulate at the disease sites, it seems more promising to use ligand molecules to target immune cells. Specific immune cells, such as monocytes, innate lymphoid cells, and T cells, along with various associated regulatory cytokines, have been extensively highlighted in the context of inflammatory bowel disease[19-21]. Furthermore, studies have pinpointed the altered trafficking of immune cell circuits as key drivers of mucosal inflammation and tissue destruction in UC[22], likening it to a severe "traffic jam" at the lesion sites. Consequently, integrins such as α4β7 and αMβ2, which are implicated in immune cell-related adhesion and signaling, could serve as excellent targets[23]. Recently, more researches tend to focus on the interference of integrin function[24], however, with little exploration of functional integrin-targeting molecules suitable for the complex gastrointestinal environment of UC. As a result, so far there is scant research on oral therapeutic systems that can specifically target inflammatory cell infiltration based on integrins.

When thinking about this issue, we noticed a polysaccharide of heparin. Heparin is an anionic polysaccharide comprising highly sulfated disaccharide units. Low molecular weight heparin (LMWH), prepared by the depolymerization of unfractionated heparin (UFH), have been recognized as attractive and have been successfully used as anticoagulants in clinical settings for several decades[25,26]. Intriguingly, due to the complex sequence of disaccharide units, where the anticoagulant fragments only account for 30 %[27], LMWH has been demonstrated to have potential beyond its anticoagulant properties and has been reported to be effective in the treatment of many other diseases, including infectious diseases, cancer and Alzheimer's disease[27-29]. More importantly, heparin is reportedly capable of serving as an adhesive ligand for integrins α4 and αM[23,30,31], known as CD49d and CD11b respectively. Inspired by these findings, we hypothesize that LMWH could be a promising inflammatory site-targeting ligand for developing precise oral therapy of UC.

Since conventional immunosuppressive drugs for UC management fail to fully address the treatment needs, it is crucial to develop groundbreaking strategies with multiple therapeutical effects for rebalancing intestinal disorders in UC. Reactive oxygen species (ROS), as an integral factor for affecting intestinal homeostasis, are signaling molecules extensively involved in numerous cellular processes[32]. However, the disproportionate generation of ROS during the UC pathogenic process, which could increase by a factor of 10 to 100[33], inflicts severe tissue damage on the intestinal epithelium and triggers the overproduction of inflammatory mediators. While small-molecule drugs have been found to have unavoidable limitations, there are mounting evidences that biocompatible polymer-based materials, typically those based on glucose-related polysaccharides, show significant potential in suppressing oxidative stress and inflammatory mediators, thereby regulating the redox balance in the colon[9,34-38]. Unfortunately, the conjunction with multiple hydroxy groups on glucose residues of the polysaccharides introduces structural uncertainty. To design optimal ROS-scavenging materials with a defined structure and well controllable function, alternative biocompatible polymers need to be explored. For instance, ε-polylysine (EPL), a cationic and biodegradable polypeptide produced by microbial fermentation, has already garnered interest in food chemistry and oral delivery systems[39]. The presence of a single amino group on each repeating unit of EPL enables the controlled modification.

Here, we strongly agree and emphasize the importance of precise nanotherapies that integrate multiple functions. Therefore, we proposed a design of modular bifunctional oral

nanotherapy, consisting of oxidation-sensitive ε-polylysine (OsEPL) nanoparticles (OPNs) as core, positively charged chitosan as middle layer and negatively charged LMWH as outmost layer, to achieve a "hitting two birds with one stone" treatment. Considering the adaptability and prospective engineering applications, we utilized nanoprecipitation and layer-by-layer self-assembly methodologies in the fabrication process. We hypothesize the oral nanoparticles not only can target to integrin-associated immune cell recruitment and trafficking due to the specific interaction between LMWH and integrin αM, but also can regulate intestinal redox homeostasis due to the ROS-scavenging function of OsEPL. Overall, we expect that our OPNs@LMWH may translate to a topical UC therapy with high patient friendliness *via* oral administration and high therapeutical efficacy as well as low side effect. Moreover, the strategy of "hitting two birds with one stone" might be a straightforward and effective approach to dealing with complex clinic problems.

Results

Preparing Integrin-targeting OPNs@LMWH by nanoprecipitation and layer-by-layer process.

The oxidation-sensitive material (OsEPL) was designed and synthesized by introducing a hydrophobic phenylboronic ester group that is sensitive to ROS into the side chain amino group, as shown in Supplementary Scheme 1 and Supplementary Fig. 1, and the intermediate and OsEPL were identified by ^{1}H NMR (Supplementary Fig. 2-4), indicating the successful synthesis. Specifically, we constructed a series of OsEPL with different feeding ratio of phenylboronic acid pinacol ester and amino. As the molar ratio of the hydrophobic side chain increased, the OsEPL gradually formed an amphiphilic polymer in aqueous phrase. Besides, OsEPL underwent rapid disintegration in when incubated with peroxide (Supplementary Fig. 5). Then we obtained OPNs and OPNs@LMWH by nanoprecipitation and layer-by-layer as illustrated in Fig. 1a. In order to obtain nanoparticles coated with LMWH, OPNs were dispersed in a chitosan buffer, which helped to form nanoparticles with positive charge layer (OPNs@CS), followed by incubating with LMWH aqueous solution for preparation of resulted OPNs@LMWH. The OPNs@LMWH presented a spherical core-shell structure with an average particle size of approximately 600 nm and low polydispersity index (PDI, less than 0.2 on average), according to scanning electron microscopy (SEM) (Fig. 1b), transmission electron microscope (TEM) (Fig. 1b, c) and dynamic light scattering (DLS) analysis (Fig. 1d). We also observed a charge-reversing between OPNs, OPNs@CS and OPNs@LMWH (Fig. 1e), which indicated the successful coating. Considering the oral administration of this nanotherapeutic, its stability within the gastrointestinal tract is a matter of concern. The stability of OPNs@LMWH was investigated by incubating them in both ddH_2O (4 °C) and simulated gastric/intestinal fluids (SGF, SIF) (Supplementary Fig. 7a). Our results demonstrated the excellent stability for store (Supplementary Fig. 7b) or after oral administration (Supplementary Fig. 7c-e).

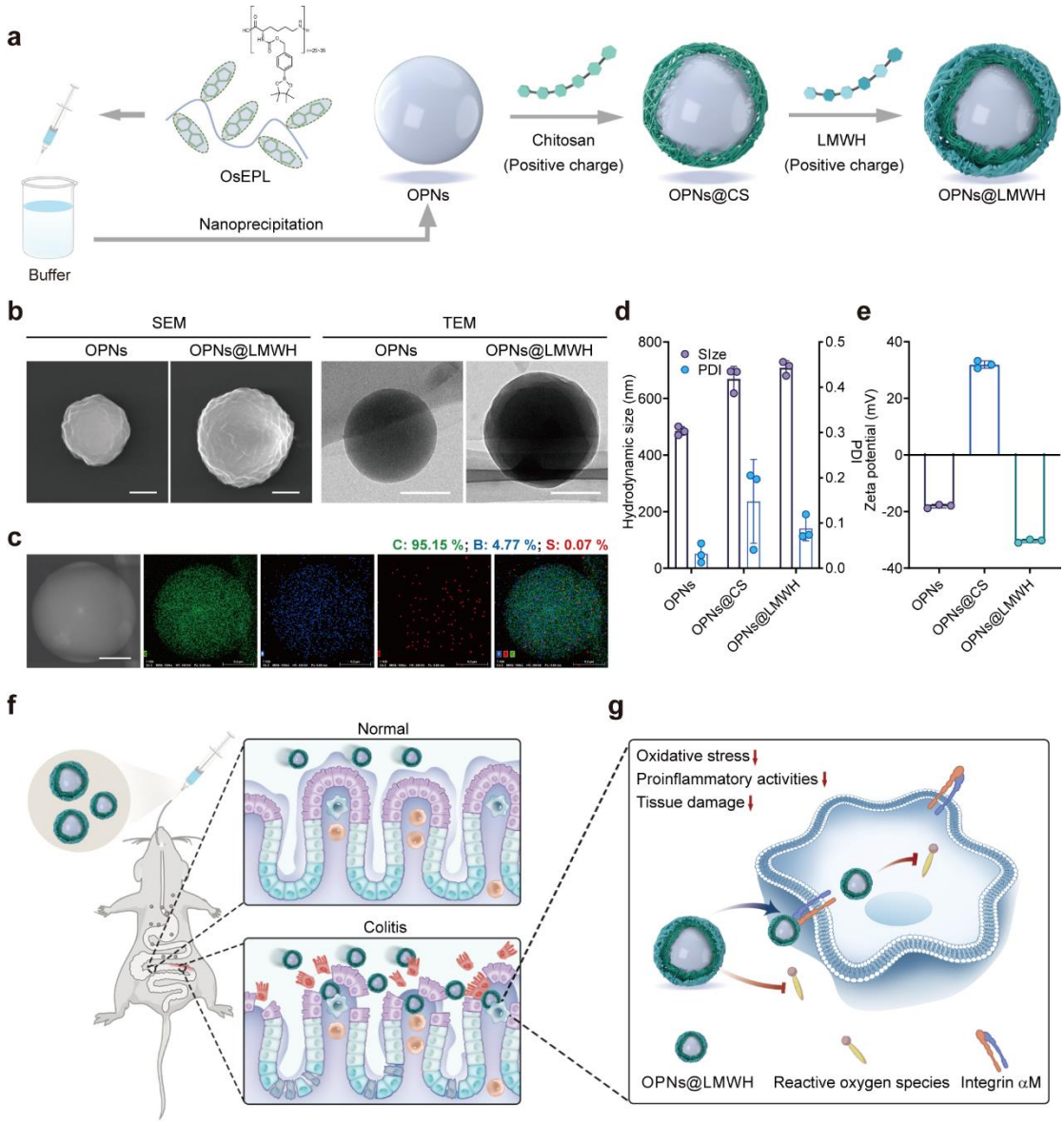

Fig. 1 | Preparation and characterization of OPNs@LMWH. a, Schematic illustration of the preparation of OPNs@LMWH. **b,** Representative SEM and TEM image of OPNs and OPNs@LMWH. Scale bar, 200 nm. **c,** C, B, S elements of OPNs@LMWH. Scale bar, 200 nm. **d, e,** Particle size (**d**) and zeta-potential (**e**) of different nanoparticles determined by DLS. Data represent mean ±SD. **f, g,** Scheme of orally administered OPNs@LMWH targeting immune cell recruitment and regulate intestinal redox homeostasis. OPNs@LMWH, when administered orally, can accumulate at the site of colitis inflammation (**f**). OPNs@LMWH achieve efficient redox homeostasis regulation by targeting the inflammation-related integrin αM (**g**).

OPNs@LMWH are internalized by M1 macrophages and accumulates in inflamed colon infiltrated by inflammatory cells.

With the establishment of preparation procedures, we next compared the efficacy of OPNs@LMWH and OPNs to be uptake by proinflammatory immune cells. To mimic the interactions between nanoparticles and proinflammatory immune cells at the lesion site,

RAW264.7 cells were activated by lipopolysaccharides (LPS) and IFN-γ to form the M1 type macrophages and then incubated with fluorescein amine (FA)-labeled OPNs (FA-OPNs) or FA-labeled OPNs@LMWH (FA-OPNs@LMWH). Then the samples were images by confocal laser scanning microscopy (CLSM), as shown in Fig. 2a and Supplementary Fig. 8. Compared with OPNs sample (untreated), OPNs@LMWH sample showed much higher green fluorescence intensity, indicating the significantly enhanced cellular uptake efficiency. Then we pretreated RAW264.7 cells with antibody against the known receptor, Integrin αM, to interfere with the potential interaction between LWMH and Integrin αM. Consistent with expectations, a reduced attachment of OPNs@LMWH was observed (Fig. 2a, b). For further illustration, we confirmed that free fluorescein was denied to access while both OPNs and OPNs@LMWH were uptake after an eight-hour incubation, which proved the enhanced cellular uptake efficiency relied on the LMWH-coating layer (Supplementary Fig. 9).

Administering drinking water containing sodium dextran sulfate (DSS) is a well-recognized method for constructing a murine model that simulates human ulcerative colitis. We adopted DSS-induced colitis mice to study the *in vivo* distribution of orally administered OPNs@LMWH. Since we have successfully confirmed the targeting of OPNs@LMWH to integrin αM *in vitro* experiments, firstly we confirmed the higher-level enrichment of integrin αM owning to the immune cell recruiting in the colonic submucosal layer of colitis mice than in normal site (Supplementary Fig. 10). As expected, we successfully observed a large accumulation of OPNs@LMWH at the lesion site *in vivo*. After orally administrated with indocyanine green (ICG)-labeled OPNs@LMWH (ICG-OPNs@LMWH), OPNs@LMWH in colitis mice presented a prolonged retention time *in vivo* and the fluorescence signal reached its peak at 12 h (Fig. 2c, d). Compared with OPNs@LMWH, naked OPNs were eliminated rapidly by both health and colitis mice (Fig. 2c, d). For colitis mice administrated with OPNs@LMWH, we also observed a significant greater accumulation in colon which presented approximately 2-fold higher than colitis mice given indocyanine green-labeled OPNs (ICG-OPNs) and 12-fold higher than other healthy mice (Fig. 2e, f). Notably, both OPNs and OPNs@LMWH were eliminated from colon in a short time by healthy mice while OPNs@LMWH were still located in the inflamed colon extensively (Fig. 2e), showing the excellent inflammation-targeting capability of OPNs@LMWH. These findings proved that OPNs@LMWH possessed integrin αM-targeting effect *in vivo*. For further observing the distribution of particles in detail, frozen sections of the colon tissue were obtained after administering FA-OPNs or FA-OPNs@LMWH for 24 h. We found that there was almost no residual fluorescence signal from the particles in normal mouse colon tissue and believed that the structurally intact intestinal barrier prevented the entry of particles and successfully excreted them (Fig. 2g, Supplementary Fig. 11). In the inflamed colon tissue, a small amount of OPNs were preserved. This could be attributed to non-specific factors such as the disruption of the intestinal barrier, the interaction between the negatively charged surface of OPNs and the positively charged inflamed mucus layer, and abnormal colon function. More significantly, a substantial amount of OPNs@LMWH not just accumulated at the site of inflammation but also penetrated deeper into the submucosal layer heavily infiltrated by integrin αM+ inflammatory cells (Fig. 2g, Supplementary Fig. 11).

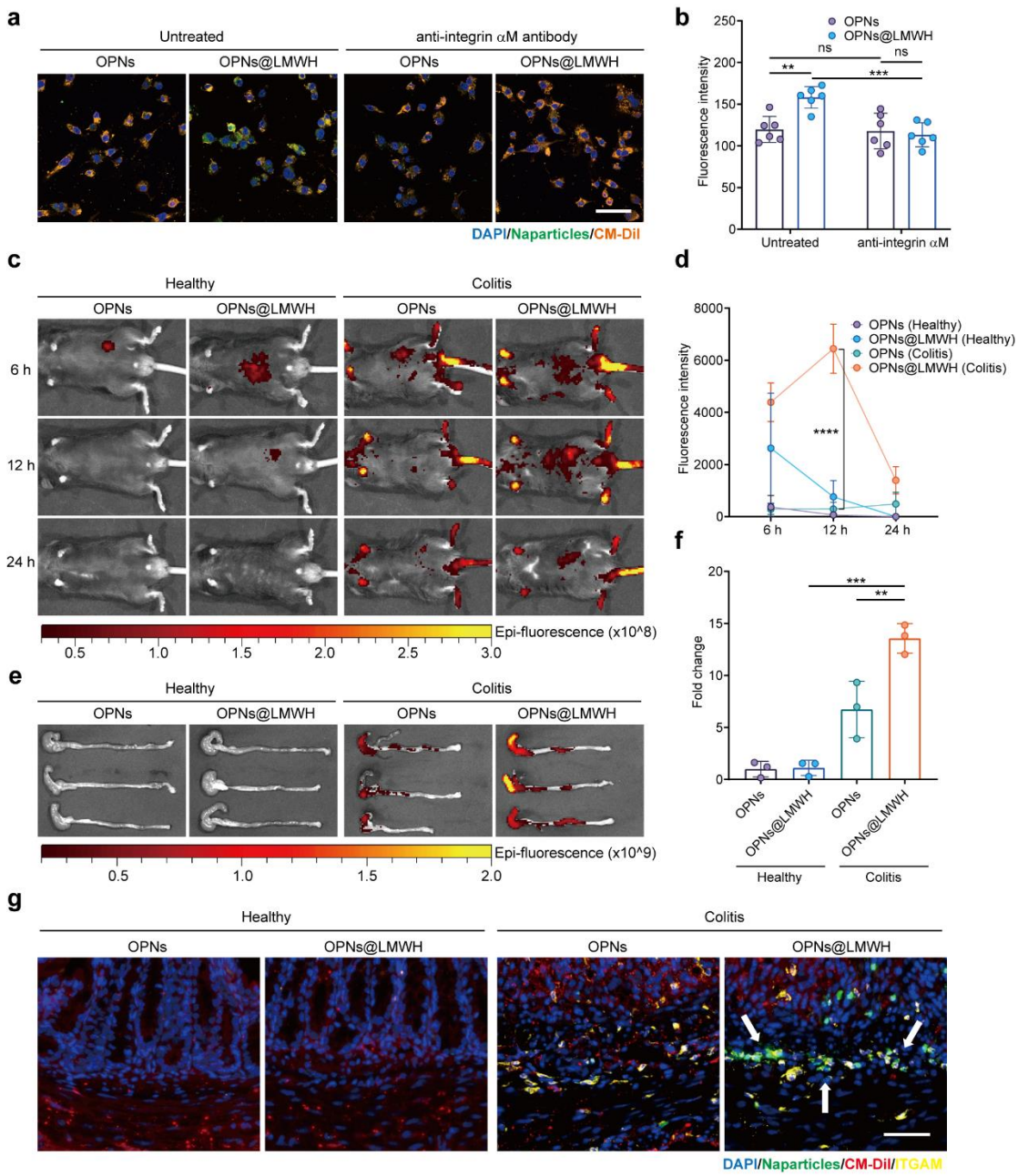

Fig. 2 | OPNs@LMWH are internalized by M1 macrophages and accumulates in inflamed colon infiltrated by inflammatory cells. a, Activated M1 type RAW264.7 cells were incubated with FA-OPNs or FA-OPNs@LMWH and pretreated with or without anti-integrin αM antibody, visualized by CLSM. Scale bar, 50 μm. **b,** Quantitative analysis of FA fluorescence intensity of images taken by CLSM. **c, d,** Representative healthy or colitis mice were orally administrated with ICG-OPNs or ICG-OPNs@LMWH, imaged by *in vivo* imaging system (IVIS) (**c**) and quantified for ICG fluorescence signal around abdomen (**d**). **e, f,** After 24 h, colons were obtained and imaged by IVIS (**e**), quantified for ICG fluorescence signal (**f**). **g,** Healthy or colitis mice were orally administrated with FA-OPNs or FA-OPNs@LMWH, and colon tissues were collected after 24 h and stained with DAPI, CM-Dil and integrin αM, visualized by CLSM. Scale bar, 50 μm. Shown are representative images or quantitative analysis of n=6 biologically independent samples (**a, b**) and n=3 animals from two independent experiments (**c-g**). Data represent mean ±SD. * $p < 0.05$, ** $p < 0.01$, *** $p < 0.001$, **** $p < 0.0001$ and ns $p > 0.05$,

analyzed by two-way ANOVA (**b, d**) or ordinary one-way ANOVA (**f**) multiple comparisons test.

Improved efficiency of OPN@LMWH against intracellular ROS and inflammation

Since the precise targeting has been proven, we next evaluated the efficacy of OPN@LMWH for immune regulation, including ROS-scavenging and anti-inflammation. First of all, a cytotoxic test was performed to illustrate the cell viability *in vitro*. The results indicated a desired biocompatibility and negligible cytotoxicity under a concentration of 100 μg/mL of nanoparticles for both macrophages and intestinal epithelial cells (Supplementary Fig. 12a-d). To investigate the ROS-scavenging behavior, RAW264.7 cells were stimulated with phorbol 12-myristate 13-acetate (PMA) and pretreated with different nanoparticles. We observed a significant concentration-dependent intracellular ROS-scavenging behavior of both OPNs and OPNs@LMWH, while OPNs@LMWH possessed a more sufficient scavenging capability due to the enhanced cellular uptake efficiency compared with others (Fig. 3a-d, Supplementary Fig. 13a-c). As a confirmatory experiment, we also found LMWH presented little anti-ROS property (Supplementary Fig. 14a-d) and the mass proportion of LMWH in OPNs@LMWH does not exceed 1 % (Supplementary Fig. 15), proving the enhanced cellular uptake efficiency rather than potential oxidative sensitivity of LMWH resulted in the enhanced intracellular ROS-scavenging behavior. Then, we evaluated the protective function provided by nanoparticles against peroxide-induced apoptosis in NCM460 cells, which represented for the extracellular ROS-scavenging behavior and the protection of intestinal epithelium. We observed a comparable result for OPNs and OPNs@LMWH (Fig. 3e, f). This result illustrated a comparable extracellular ROS-scavenging behavior. Surprisingly, OPNs could also suppress the production of both IL-6 and TNF-α, which are two essential proinflammatory cytokines in most of the autoimmune diseases. This function was also improved by LMWH-coating (Fig. 3g, h). Considering the mutually reinforcing relationship between oxidative stress and inflammation, we attribute this improvement on anti-inflammation to increased cellular uptake and the consequent increase in intracellular ROS-scavenging efficiency, where LMWH played an important part. These results demonstrated OPNs@LMWH is more effective in comprehensively reversing the situation of oxidative stress and inflammation.

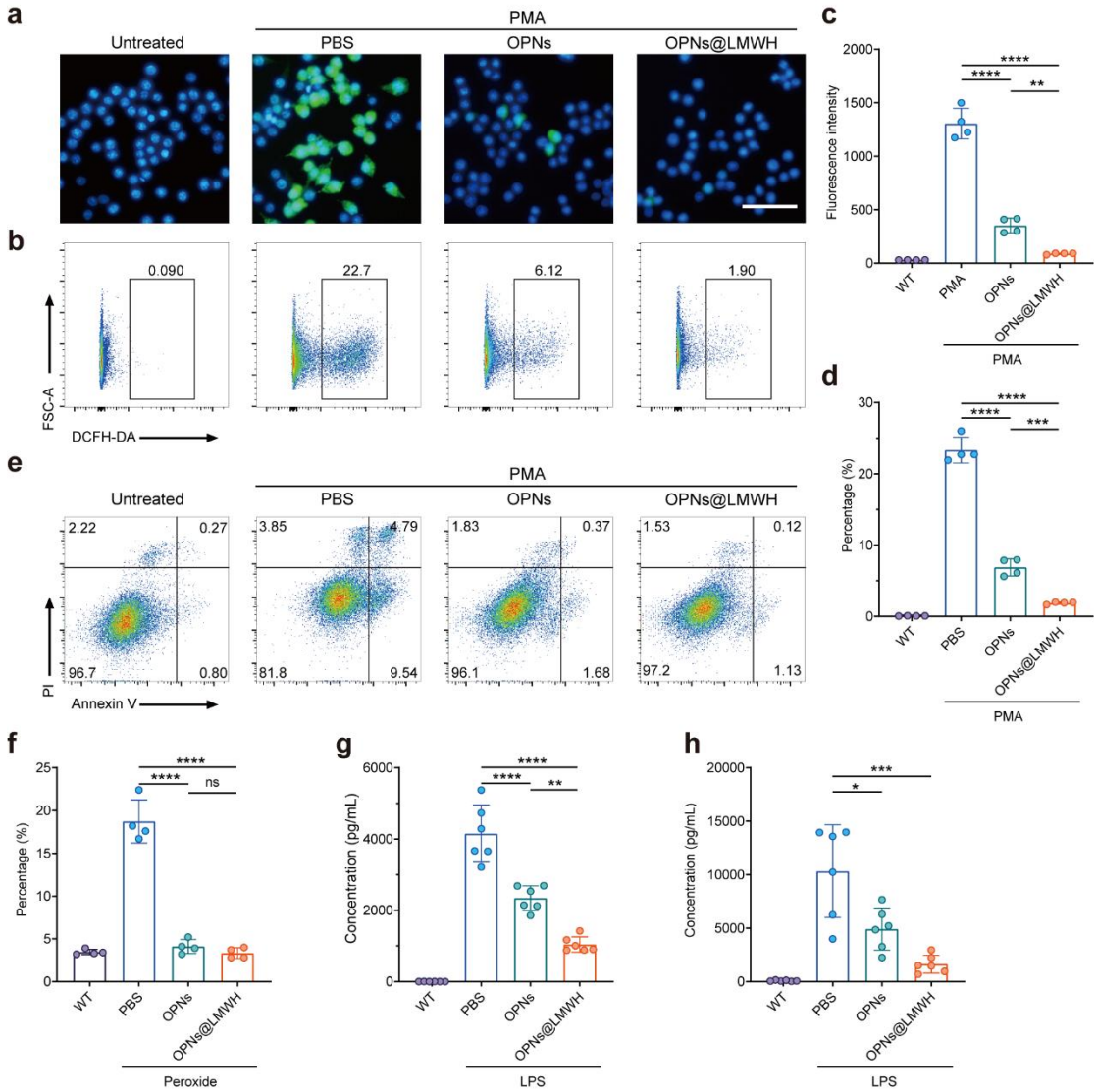

Fig. 3 | OPNs@LMWH possess enhanced intracellular ROS-scavenging and proinflammatory cytokines production. a-d, RAW264.7 cells were stimulated with PMA and treated with OPNs or OPNs@LMWH (10 μg/mL). The level of intracellular ROS was detected by DCFH-DA, visualized by Fluorescence microscope (**a**) and determined by flow cytometry (**b**). Fluorescence intensity (**c**) and percentage of ROS-positive cell were calculated (**d**). **e, f,** NCM460 cells were incubated with H_2O_2 (500 μM) and treated with OPNs or OPNs@LMWH (10 μg/mL). Peroxide-induced apoptosis was detected by staining with Annexin-V and PI (**e**). Total apoptosis percentages of different treatments were calculated (**f**). **g, h,** RAW264.7 cells were stimulated with LPS to produce proinflammatory cytokines and incubated with OPNs or OPNs@LMWH (10 μg/mL). The concentration of IL-6 (**g**) and TNF-α (**h**) were determined by ELISA. Shown are representative images, gating strategy or quantitative analysis from n=4 biologically independent samples (**a-f**) and n=6 biologically independent samples (**g, h**). Data represent mean ±SD. * $p < 0.05$, ** $p < 0.01$, *** $p < 0.001$, **** $p < 0.0001$ and ns $p > 0.05$, analyzed by ordinary one-way ANOVA (**c, d, f-h**) multiple comparisons test.

Therapeutic efficacy evaluation of OPNs@LMWH for UC treatment by oral administration

We next investigated the therapeutic efficacy of OPNs@LMWH in alleviating the manifestations of colitis in mice. We first examined the *in vivo* safety of OPNs@LMWH to confirm that a high dose constant daily oral administration in two weeks will not present a significant damage to mice. Our results indicated there is no evidence-based damage observed in five main organs after the constant daily oral administration with different concentrations, which proved for the ideal preliminary biosafety (Supplementary Fig. 16-18). Then we investigated the therapeutic outcomes of OPNs and OPNs@LMWH for colitis mice. Fig. 4a schematically showed the DSS-induced colitis mouse model development and the oral treatment strategies based on OPNs or OPNs@LMWH. Compared with water, both OPNs and OPNs@LMWH significantly protected mice against colitis, and body weight loss (Fig. 4b), shortening of colon length (Fig. 4c, e) and enlarging of spleen (Fig. 4d, f). Importantly, compared with naked-OPNs, there was a significant improving that has been observed for OPNs@LMWH. According to the histopathological examination, treating with OPNs@LMWH also protected colonic epithelium against pathological damage and the structure of crypts were significantly completer and more stable (Fig. 4g, h). These results indicated OPNs@LMWH could effectively alleviate disease status and LMWH-coating could significantly improve the efficiency, which were consistent with in vitro experiments and our speculation.

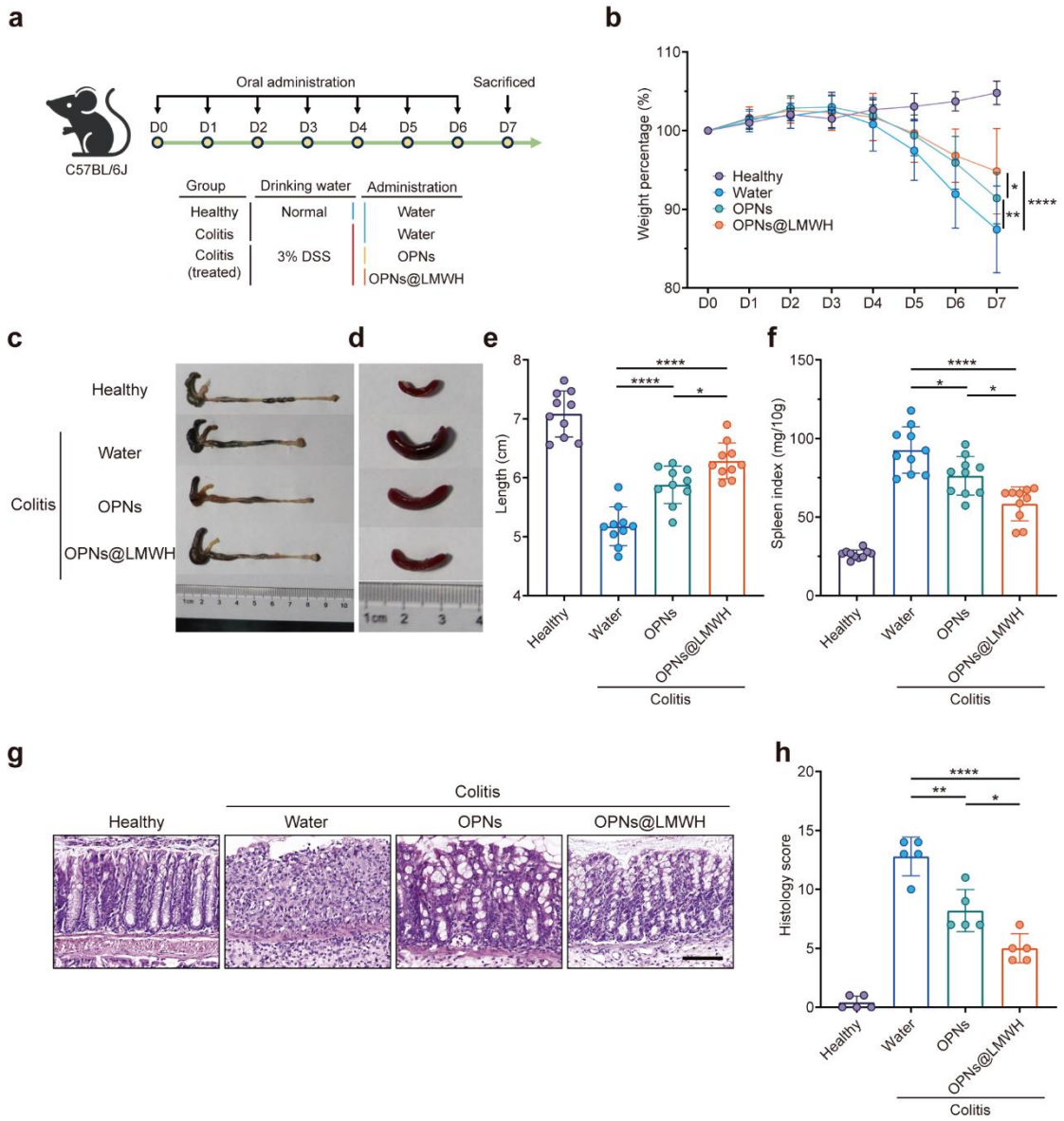

Fig. 4 | Therapeutic efficacy evaluation of OPNs@LMWH for colitis mice. a, Schematic illustration of DSS-induced colitis mouse model development. Mice were daily administrated with 50 mg/kg of OPNs, OPNs@LMWH or drinking water. **b,** Daily bodyweight changes in each group. **c-f,** Mice were scarified on day 7 and colon (**c**) and spleen (**d**) were collected. Colon length (**e**) and Spleen index (**f**) were quantitated. **g,** Representative images of colons stained with Hematoxylin and eosin. Scale bar, 100 μm. **h,** Histology score was evaluated to quantitated tissue damage. Shown are representative images or quantitative analysis from n= 10 animals (**b-f**) and n=5 biologically independent samples (**g, h**). Data represent mean ±SD. * $p < 0.05$, ** $p < 0.01$, *** $p < 0.001$, **** $p < 0.0001$ and ns $p > 0.05$, analyzed by two-way ANOVA (**b**) or ordinary one-way ANOVA (**e, f, h**) multiple comparisons test.

OPNs@LMWH restores intestinal homeostasis and protects colonic epithelium.

Our results described above had revealed the potential of OPNs@LMWH in restoring intestinal redox homeostasis. Inspired by these results, we examined the mechanisms of OPNs@LMWH for UC management. Our results of Enzyme linked immunosorbent assay

305 (ELISA) confirmed lower levels of proinflammation cytokines in both peripheral blood and
306 lamina propria of colitis mice treated with OPNs@LMWH compared with pure water and
307 OPNs (Fig. 5a-d). These results fully revealed the enhanced immune regulation ability of
308 OPNs@LMWH compared with OPNs. According to the evaluation by immunohistochemical
309 (IHC) staining with myeloperoxidase (MPO), we observed a lowest oxidative stress in the colitis
310 colon with OPNs@LMWH treatment compared with other groups. Remarkably, the decrease
311 in the proportion of MPO-positive cells for OPNs@LMWH treatment was primarily attributed
312 to a significant reduction in the submucosal layer, which is rich of recruited proinflammatory
313 immune cells (Fig. 5e). This result indicated that OPNs@LMWH precisely influenced the
314 production of excess pro-inflammatory cytokines in immune cells through ROS-scavenging,
315 which is consistent with our results *in vitro*. According to IHC results, we also observed a
316 decreased activation of JAK-STAT signaling pathway in lamina propria after OPNs@LMWH
317 treatment (Fig. 5f). As an essential signaling transduction pathway, JAK-STAT is mainly
318 activated by proinflammatory cytokines in colitis lesion, hence, the decreased activation of
319 which indicated a reduction in overall inflammatory activity.
320 An important sign of restoration of intestinal homeostasis is the normalization of crypt
321 maintenance and self-renewal. The stability and rapid renewal of the intestinal mucosal layer
322 depend on the orderly arrangement of crypt cells and the performance of each functional cell,
323 including maintaining the epithelial barrier and regulating cell proliferation and apoptosis[40].
324 By immunofluorescence staining, we interestingly found epithelial cells was restored and
325 arranged more regularly in colitis mice treated with OPNs@LMWH, which also indicated that
326 intestinal mucosal permeability was restored (Fig. 5g, h). We utilized the cleaved caspase 3
327 (CC3), a marker of apoptosis, to investigate the occurrence of apoptosis in colitis mice. Our
328 findings revealed a substantial overlap between cells exhibiting high expression of CC3 and
329 E-cadherin in colitis mice without treatment (Fig. 5h, i, k). Concurrently, the proliferation
330 (marked by PCNA) of transit amplifying (TA) cells and intestinal stem cells located at the base
331 of the crypts was virtually halted (Fig. 5j). This suggests that the mucosal layer in colitis has
332 lost its barrier and self-repair capabilities. However, for colitis mice treated with OPNs and
333 OPNs@LMWH, a significant reduction in the proportion of apoptotic epithelial cells was
334 observed, demonstrating the proliferation of crypt cells was reinstated (Fig. 5i-k). More
335 importantly, most of the PCNA-positive cells were gathered at the bottom of the crypts after
336 the effective treatment. This result indicated that the restored proliferation ensured orderly
337 proliferation and differentiation (Fig. 5j). Taken together, these findings proved that
338 OPNs@LMWH can significantly remit the UC *in vivo* by maintaining the redox and immune
339 homeostasis, as well as protecting the colonic epithelium.

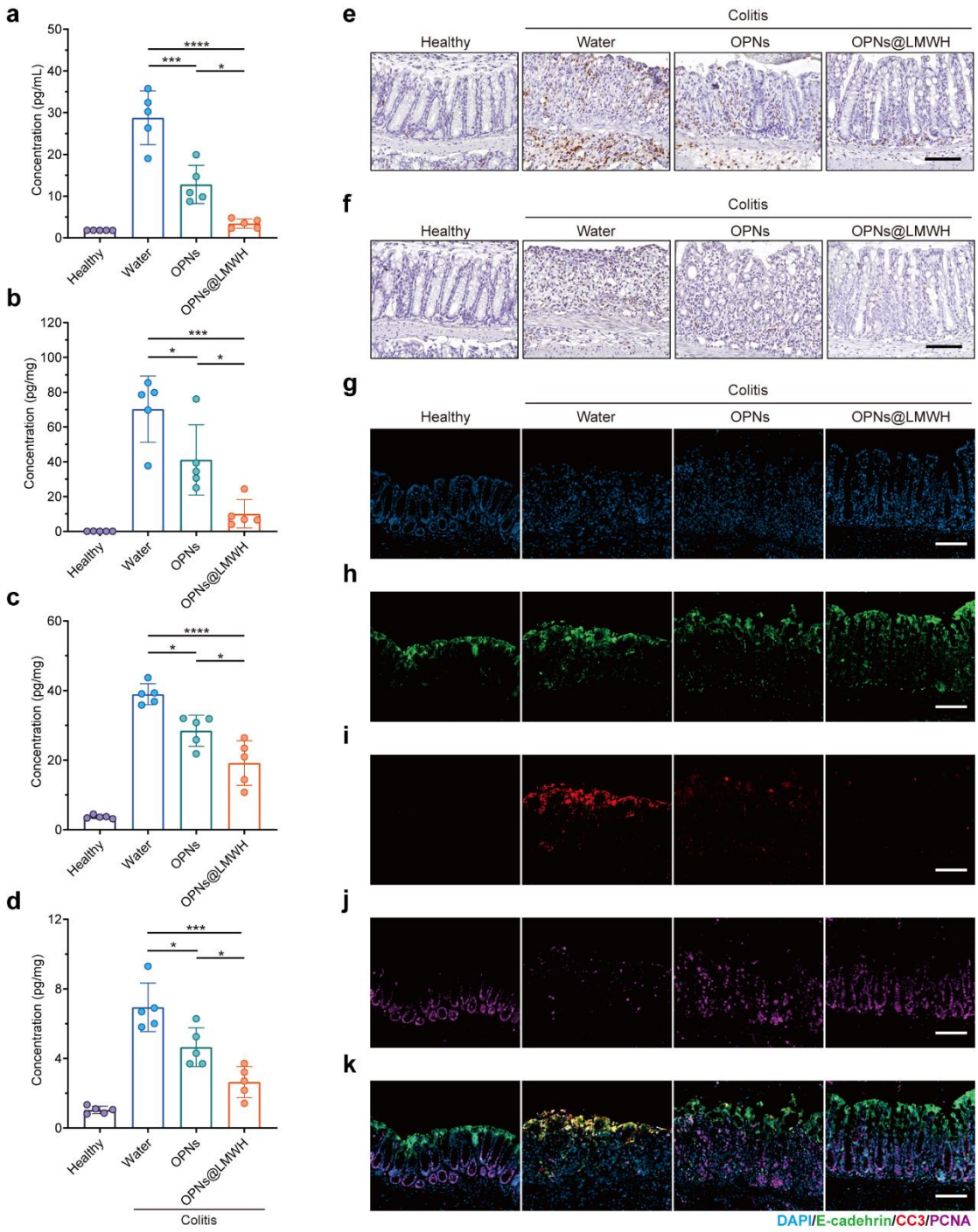

Fig. 5 | The rebalanced intestinal homeostasis after treated with OPNs@LMWH. a-d, Colitis mice were treated with OPNs or OPNs@LMWH. The concentration of IL-6 in serum (**a**) and IL-6 (**b**), TNF-α (**c**) and IL-1β (**d**) in colon tissue were determined by ELISA. **e, f,** Representative images of immunohistochemical staining for MPO (**e**) and p-STAT3 (**f**). Scale bar, 100 μm. **g-k,** Representative images of immunofluorescence staining for proliferation and apoptosis, presented with DAPI (**g**), anti-E-cadherin (**h**), anti-PCNA (**i**), anti-CC3 (**j**) and merge (**k**), visualized by CLSM. Scale bar, 100 μm. Shown are quantitative analysis or representative images from n= 5 biologically independent samples (**a-d**) and n= 3 biologically independent samples (**e-k**). Data represent mean ±SD. * $p < 0.05$, ** $p < 0.01$, *** $p < 0.001$, **** $p < 0.0001$ and ns $p > 0.05$, analyzed by ordinary one-way ANOVA (**a-d**)

multiple comparisons test.

Discussion

The intricacies of ulcerative colitis present significant challenges for existing treatment methods. Current clinical drugs have notable limitations, and off-target effects from oral medications are concerning[8,41]. To address this issue, numerous studies have been conducted on precision drug delivery systems for ulcerative colitis, yielding promising results[11,12]. Despite varying approaches and outcomes in previous research, there is consensus that designing multifunctional targeted new therapies for immune response holds great potential[18].

Our work considered the transport and infiltration phenomena of inflammatory cells at ulcerative colitis lesion sites and proposed a "hitting two birds with one stone" precise nanotherapy based on integrin αM-targeting and ROS-scavenging. Adopting a modular integration approach, OsEPL was combined with LMWH through nanoprecipitation and layer-by-layer self-assembly to form core-shell nanoparticles. Given the imbalance of redox homeostasis at inflammation sites, we opted for a drug-free approach using biocompatible ROS-scavenging materials derived from modified ε-polylysine as a regulator for intestinal oxidative stress.

Despite the discovery of the heparin-integrin interaction mechanism in existing research, our knowledge regarding its potential in drug delivery remains sparse. Our findings robustly validated an enhanced immune cellular uptake of heparin-coated nanoparticles and highlights the crucial mediating role of LMWH-integrin αM interactions. As anticipated, OPNs@LMWH successfully targeted intestinal inflammatory cell migration, accumulation, and infiltration in colitis mice. OPNs@LMWH demonstrated a significantly extended retention time in the colon of colitis mice. Remarkably, 24 hours post-oral administration, the concentration was approximately double compared to that of the naked form. Conversely, normal mice rapidly eliminated OPNs@LMWH, underscoring its superior inflammation-targeting properties and minimized potential adverse effects. A closer examination of colon tissue sections revealed that OPNs@LMWH penetrated more deeply into the submucosal tissues with inflammatory cell infiltration, compared to OPNs, further highlighting its enhanced inflammation-targeting efficiency.

To understand how OPNs@LMWH improves colitis, we conducted comprehensive in vivo and in vitro experiments to investigate its impact. In our in vitro studies, we noted a reduction in the levels of intracellular ROS and pro-inflammatory cytokine secretion following the application of OPNs@LMWH. Interestingly, in experiments involving cells damaged by exogenous peroxides, the performance of OPNs@LMWH was comparable to that of OPNs. These findings suggest that while the cellular uptake efficiency of OPNs@LMWH has been enhanced, its inherent antioxidant functionality remains effective. In subsequent *in vivo* trials, OPNs@LMWH demonstrated superior effectiveness in alleviating the symptoms of colitis. Our results revealed that following treatment with OPNs@LMWH, there was a significant reduction in the levels of peripheral blood and inherent inflammatory responses in mice with colitis. Additionally, we noted a marked decrease in oxidative stress levels within immune cells and a diminished activation of the JAK-STAT signaling pathway. The process of apoptosis in the intestinal epithelial cells of the mice was effectively suppressed, and the structured proliferation at the base of the crypts was successfully reinstated.

Our findings provide robust validation for our "hitting two birds with one stone" strategy that combines LMWH-based integrin targeting with the regulation of intestinal redox homeostasis, thereby highlighting the application of OPNs@LMWH in the treatment of ulcerative colitis. More promisingly, our research underscores the feasibility and flexibility of employing LMWH in integrin-targeted treatment strategies for ulcerative colitis *via* oral administration. We postulate that the LMWH surface coating could be universally implemented across a variety of nanoparticle designs targeting integrins α4 and αM. This straightforward and adaptable modular design could potentially stimulate further research into integrin-targeted treatment strategies for autoimmune diseases.

Experimental section

Materials:

ε-polylysine, 4-hydroxyphenyl boronic acid pinacol ester, dichloromethane (DCM), carbonyl diimidazole (CDI), Sodium chloride (NaCl), Sodium sulfate (Na_2SO_4), 4-dimethylaminopyridine (DMAP), dimethyl sulfoxide (DMSO), lecithin, ammonium acetate (CH_3COONH_4) and Hydrogen peroxide solution (H_2O_2) were purchased from Aladdin (Shanghai, CHN). Heparin was purchased from Changshan Biotechnology Co. Ltd (Hebei, CHN). Chitosan (CS, >75% deacetylated), Indocyanine green (ICG), fluorescein amine (FA), Azure A, Lipopolysaccharides (LPS), Phorbol 12-myristate 13-acetate (PMA), sucrose and hematoxylin solution were purchased from Sigma–Aldrich (St. Louis, MO, USA). Cell counting kit-8, BCA Protein Assay Kit, Protease and phosphatase inhibitor cocktail for mammalian cell and tissue extracts (P1050) and DCFH-DA were purchased from Beyotime Biotechnology (Shanghai, CHN). Fetal bovine serum (FBS) was purchased from Gemini (USA). Dulbecco's modified Eagle's medium (DMEM), Roswell Park Memorial Institute (RPMI) 1640 medium, Opti-MEM I reduced serum medium were purchased from Gibco (USA). Dextran sulfate sodium (DSS, colitis grade) was purchased from MP Biomedicals (USA). Anti-E-cadherin antibody (14-3249-82), CM-DiI (C7001) and ELISA kits IL-6 (88-7064), TNF-α (88-7324), IL-1β (88-7013) were purchased from Invitrogen (USA). Annexin-V/PI kit was purchased from BioLegend, Inc. (USA). Antibodies anti-phospho-Stat3 (Tyr705, 9145), anti-cleaved caspase-3 (Asp175, 9579) and anti-PCNA (2586) were purchased from Cell Signaling Technology (USA). Antibodies anti-myeloperoxidase (ab208670) and anti-integrin αM (ab133357) were purchased from Abcam (Cambridge, UK). DAPI was purchased from Thermo Scientific (USA). Secondary antibodies conjugated with Alexa Fluor 488 (A-21208), 594 (A-21207), 647 (A-31573 and A-31571) were purchased from Invitrogen (USA). Secondary antibodies conjugated with horseradish peroxidase (HRP), 3,3'-diaminobenzidine (DAB), peroxidase-blocking solution and serum-free protein blocking solution were purchased from Dako (DNK). O.C.T. compound was purchased from Sakura (USA).

Synthesis of OsEPL: Oxidation-sensitive ε-polylysine (OsEPL) were synthesized by using a method inspired by K. E. Broaders & et al[42] with modification. Briefly, 4-hydroxyphenyl boronic acid pinacol ester (10 mmol) was dissolved in DCM (10 mL). Then CDI (20 mmol) was added and the mixture was stirred at R.T. for 1 h. The solution was diluted by adding another 10 mL DCM and washed with dd-H_2O (20 mL) three times. Then the obtained organic phrase was washed with saturated brine (20 mL) three times, dried over anhydrous Na_2SO_4 for 30 min

439 and concentrated in a rotary evaporator to obtain imidazoyl carbamate (Compound 1, 8.5
440 mM, 85%). To form OsEPL, Compound 1 (820 mg), ε-polylysine (320 mg) and DMAP (305 mg)
441 were dissolved in anhydrous DMSO (10 mL). The mixture was stirred at R.T. for 24 h. Then
442 OsEPL was precipitated in dd-H_2O (40 mL) and isolated by centrifugation (8000 g, 10 min).
443 The precipitate was washed with dd-H_2O (20 mL) three times and lyophilized for further use.
444
445 **Preparation of OPNs@LMWH:** LMWH (Mw=8.5kDa) was prepared by a controlled
446 heparinase depolymerization method according to reports.[26,43] The molecular weight of
447 unfractionated heparin (UFH) and LMWH were determined by HPLC (1260 Infinity II, Agilent,
448 USA) with a GPC column (TSK Gel G2000SWXL, 7.8 mm × 300 mm, Tosoh Co., JPN) and the
449 result is shown in Supplementary Fig. 6. OPNs@LMWH were prepared by a
450 nanoprecipitation/layer-by-layer method. Briefly, lecithin (20 mg) was dispersed in 1 mL
451 anhydrous ethanol and then added dropwise to 8 mL CH_3COONH_4 buffer (0.1 M, pH = 5.00)
452 with magnetic stirring (600 rpm) to form a dispersion. OsEPL (20 mg) was dissolved in DMSO
453 (1 mL) and then added dropwise to the dispersion. The nanoparticles were collected by
454 centrifugation (30000 g, 10 min). Naked OPNs were harvested after washing three times with
455 dd-H_2O. Chitosan (20 mg) was dissolved in 10 mL CH_3COONH_4 buffer (0.1 M, pH = 5.00).
456 Then the Nanoparticles were dispersed in the chitosan solution and incubated at R. T. for 30
457 min with magnetic stirring (600 rpm). The chitosan-coated OPNs were collected after washed
458 three times with dd-H_2O, dispersed in 10 mL LMWH aqueous solution (2 mg mL^{-1}) and
459 incubated at R. T. for 30 min with magnetic stirring (600 rpm) again. Finally, OPNs@LMWH
460 were washed three times either and collected by centrifugation (30000 g, 10 min) for further
461 use. For *in vivo* imaging applications, ICG (1 mg mL^{-1}) or FA (1 mg mL^{-1}) was added to the
462 primary DMSO solution and two kinds of fluorescent labeled OPNs or OPNs@LMWH were
463 prepared by a similar method to the above. The fluorescence intensity of fluorescent labeled-
464 nanoparticles was normalized before use.
465
466 **Characterization of OPNs@LMWH:** The surface morphology of OPNs and OPNs@LMWH
467 were determined by SEM (Merlin, Zeiss, DEU), TEM (Tecnai G2 20, FEI, USA) and AC-TEM
468 (Titan 80-300, FEI, USA). The size, polydispersity index (PDI) and surface charge of OPNs and
469 OPNs@LMWH were analyzed by DLS (Zetasizer Nano ZS90, Malvern, UK). For stability assays,
470 simulated gastric fluid (SGF) and simulated intestinal fluid (SIF) were prepared guided by
471 United States Pharmacopeia. Nanoparticles were dispersed and incubated in deionized water
472 (48 h) in 4 °C or SGF (2 h) and SIF (44 h) in 37 °C. Degradation was evaluated by examining
473 the absorbance at 500nm by microplate reader (Infinite M200 Pro, Tecan Trading AG,
474 Switzerland). The mass proportion of LMWH in OPNs@LMWH was determined indirectly by
475 measuring the concentration of free LMWH in the supernatant before and after coating. The
476 concentration of LMWH was detected by incubated with Azure A.
477
478 **Cell culture:** RAW264.7 (mouse) macrophages and NCM460 (human) colonic enterocytes
479 were kindly provided by Prof. Zhijie Chang (School of medicine, Tsinghua University, China).
480 RAW264.7 was kept in DMEM with 10 % FBS, NCM460 was kept in RPMI 1640 medium with
481 10% FBS. For in vitro assays, mediums were replaced with Opti-MEM I reduced serum
482 medium after seeded overnight to avoid potential impacts from FBS.

In vitro cellular uptake assays: RAW264.7 was seeded in 12-wells plate (Corning 3513, USA) with a density of 3 × 10^5 cells per well and stimulated with LPS (100 ng mL^{-1}) and IFN-g (20 ng mL^{-1}) for 12 h. Then FA-labeled nanoparticles with a concentration of 20 μg mL^{-1} were added. After an 8 h incubation, cells were collected and washed with PBS three times. The fluorescence intensity of cells was immediately assessed by flow cytometry (LSRFortessa, BD, USA). To confirm the improved cellular uptake efficiency, free FA with the same fluorescence intensity as nanoparticles was occupied as a control group. For immunofluorescence imaging, cells were seeded on round coverslips and pretreated with anti-integrin αM antibodies for 1h before the 8 h incubation with nanoparticles. Cells on coverslips were fixed in 4 % paraformaldehyde for 15 min, stained with CM-Dil and DAPI and washed three times. Images were performed by a confocal laser scanning microscopy (FV3000RS, Olympus, JPN).

In vitro ROS-scavenging behaviors and anti-inflammation assays: Intracellular ROS level was evaluated by a DCFH-DA method. Briefly, RAW264.7 was seeded in 12-wells plate (Corning 3513, USA) with a density of 3 × 10^5 cells per well. After incubation for 12 h, the medium was replaced with Opti-MEM containing Nanoparticles with certain concentration and incubated for another 12 h. Then PMA (100 ng mL^{-1}) and DCFH-DA were added. After incubation for 1 h, cells were all collected and washed with PBS three times. The fluorescence intensity of cells was immediately assessed by flow cytometry. To confirm the ROS-scavenging function, reduction on peroxide-induced apoptosis was evaluated by a Annexin-V/PI method. Briefly, NCM460 was seeded in 12-wells plate (Corning 3513, USA) with a density of 3 × 10^5 cells per well. After incubation for 12 h, the medium was replaced with Opti-MEM containing Nanoparticles (10 μg mL^{-1}) and incubated for 1h. Then H_2O_2 (500 μM) was added and the plate was incubated for 12 h. Then cells were collected, stained by using Annexin-V/PI apoptosis kit and assessed by flow cytometry immediately. For in vitro anti-inflammation assay, RAW264.7 was seeded in 96-wells plate (Corning 3599, USA) with a density of 3 × 10^4 cells per well. After incubation for 12 h, the medium was replaced with Opti-MEM containing LPS (100 ng mL^{-1}). After stimulated with LPS for 30 min, nanoparticles with certain concentration (10 μg mL^{-1}) were added and cells were incubated for 24 h. The supernatant was collected to determine the concentration of proinflammatory cytokines by ELISA kit.

Animals and colitis model: All animal studies were in compliance with the regulations of Laboratory Animal Resources Center, Tsinghua University (23-XXH2). Six-week-old male C57BL/6J mice were obtained from Charles River (Beijing, CHN) and maintained in a 12 h light-dark cycle at 25 °C. Mice supplied with food and water were cohoused for 7 days before random assignment to experimental groups. Colitis model was established by providing drinking water containing 3% DSS and the special drinking water was renewed every other day.

In vivo therapeutic efficacy: Mice were orally administrated with drinking water or nanoparticles dispersions at a dose of 50 mg kg^{-1} d^{-1} every day for 6 days, starting on the day 1. On day 7, Mice were sacrificed and spleens, colons and serum were excised. To obtain

histological sections, colons were fixed in 4 % paraformaldehyde for 24 h, dehydrated and embedded in paraffin. The samples were cut into 5 μm thick slides by using a microtome (RM2235, Leica, DEU) and stored in -20 °C for further use. Hematoxylin and eosin staining was performed to evaluate histopathology. The histological scores were evaluated refer to a reported method[44] with modification. Briefly, infiltration of inflammatory cells (0: none, 1: mild, 2: moderate, 3: severe), the depth of ulceration involvement (0: none, 1: mucosa, 2: submucosa, 3: muscular layer), the area of ulceration involvement (0: none, 1: 0 %–25 %, 2: 26 %–50 %, 3: 51 %–75 %, 4: 76 %–100 %), and crypt destruction (0: none, 1: lower than one third, 2: lower than two thirds, 3: more than two thirds, 4: all crypts and epithelium) were assessed. To determine the concentrations of cytokines in colon tissues, colon segments were homogenized (30 Hz, 2 min) in PBS containing 2 % protease and phosphatase inhibitor cocktail. The supernatants were collected and cytokines were assessed by ELISA kits. All samples were normalized to equivalent protein concentrations by using a BCA protein assay kit.

Immunohistochemistry and immunofluorescence imaging: Immunohistochemistry (IHC) and Immunofluorescence (IF) were applied to investigate the mechanisms. Briefly, histological sections were obtained by the same method as "In vivo therapeutic efficacy" part and followed with deparaffinization and hydration of tissue slides through xylene and gradient ethanol treatment, respectively. Antigen retrieval was performed at 100 °C for 15 min in Tris-EDTA buffer (pH = 9.00). For IHC, a peroxidase-blocking solution was applied to eliminate non-specific staining, while for IF, a serum-free protein blocking solution was applied. Tissue slides were incubated overnight at 4 °C with primary antibodies. All slides were washed with PBS (containing 0.05 % Tween-20) and incubated with secondary antibodies for 30 min at R.T., where antibodies conjugated with HRP were used in IHC and antibodies conjugated with fluorescence were used in IF. For IHC, DAB was applied to develop the color, followed by hematoxylin staining. For IF, Nucleus staining was performed by using DAPI. Then, all slides were mounted with mounting medium (Leica), protected from light and stored at 4 °C.

In vivo biodistribution: Both healthy mice and mice with colitis were investigated and orally administrated with fluorescent labeled OPNs/OPNs@LMWH. Briefly, after fasted overnight, mice orally administrated with ICG-OPNs/OPNs@LMWH were imaged by an IVIS unit (Lumina III, USA) at 6 h, 12 h and 24 h after gavage, and then sacrificed to perform colon imaging. To investigate the specific distribution in colon tissue, mice orally administrated with FA-OPNs/OPNs@LMWH were sacrificed at 24 h after gavage. Colons were obtained and stored in PBS containing 30% sucrose for 24 h. Then the solution was removed and all samples were embedded in O.C.T. compound. Histological sections were obtained by used freezing microtome (CM3050S, Leica, DEU). Slides were stained with DAPI and CM-DiI, mounted, protected from light and stored in 4 °C.

Safety assays: In vitro safety assays were based on cells. Briefly, cells were cultured in 96-wells plates with different concentrations of particles for 24 h. Then CCK-8 were added and plates were incubated for another 30 min. The absorbance at 450 nm in each well was read and used to calculate cell viability. In vivo safety assays were based on mice. Briefly, mice were daily orally administrated for 14 days with different dose of nanoparticles and their body

weights were recorded every day. Then all mice were sacrificed on Day 14. The blood samples were collected and used for blood hematology examination. The spleens, hearts, lungs, livers and kidneys of mice were collected to obtain sections and stained with hematoxylin and eosin.

Statistical analysis: The data are expressed as the mean ± standard deviation (SD). Statistical analysis was performed by student's t tests for unpaired data and by one-way ANOVA or two-way ANOVA analysis for multiple comparisons. A two tailed P value of < 0.05 was considered statistically significant and statistical significance is indicated as * $p < 0.05$, ** $p < 0.01$, *** $p < 0.001$, **** $p < 0.0001$ and ns (no significance) $p > 0.05$. GraphPad Prism 8.3 software was applied for statistical analysis.

References

1 Kobayashi, T. *et al.* Ulcerative colitis. *Nat. Rev. Dis. Primers.* **6**, 74 (2020).

2 Ungaro, R., Mehandru, S., Allen, P. B., Peyrin-Biroulet, L. & Colombel, J. F. Ulcerative colitis. *Lancet* **389**, 1756-1770 (2017).

3 Kaplan, G. G. & Ng, S. C. Understanding and preventing the global increase of inflammatory bowel disease. *Gastroenterology* **152**, 313-321 .e312 (2017).

4 Raine, T. *et al.* ECCO Guidelines on Therapeutics in Ulcerative Colitis: Medical Treatment. *J. Crohns Colitis* **16**, 2-17 (2022).

5 Ko, C. W. *et al.* AGA Clinical Practice Guidelines on the Management of Mild-to-Moderate Ulcerative Colitis. *Gastroenterology* **156**, 748-764 (2019).

6 Feuerstein, J. D. *et al.* AGA Clinical Practice Guidelines on the Management of Moderate to Severe Ulcerative Colitis. *Gastroenterology* **158**, 1450-1461 (2020).

7 Bernstein, C. N. *et al.* World gastroenterology organization practice guidelines for the diagnosis and management of IBD in 2010. *Inflamm. Bowel. Dis.* **16**, 112-124 (2010).

8 Matsuoka, K. *et al.* Evidence-based clinical practice guidelines for inflammatory bowel disease. *J. Gastroenterol.* **53**, 305-353 (2018).

9 Shi, C. *et al.* A nanoparticulate dual scavenger for targeted therapy of inflammatory bowel disease. *Sci. Adv.* **8**, eabj2372 (2022).

10 Tabas, I. & Glass, C. K. Anti-Inflammatory therapy in chronic disease: challenges and opportunities. *Science* **339**, 166-172 (2013).

11 Awad, A. *et al.* Clinical translation of advanced colonic drug delivery technologies. *Adv. Drug Deliv. Rev.* **181**, 114076 (2022).

12 Duran-Lobato, M., Niu, Z. & Alonso, M. J. Oral delivery of biologics for precision medicine. *Adv. Mater.* **32**, 1901935 (2020).

13 Bertoni, S. *et al.* pH and reactive oxygen species-sequential responsive nano-in-micro composite for targeted therapy of inflammatory bowel disease. *Adv. Funct. Mater.* **28**, 1806175 (2018).

14 Ding, Y. F. *et al.* Oral colon-targeted konjac glucomannan hydrogel constructed through noncovalent cross-linking by cucurbit 8 uril for ulcerative colitis therapy. *ACS Appl. Bio Mater.* **3**, 10-19 (2020).

15 Neurath, M. F. & Travis, S. P. L. Mucosal healing in inflammatory bowel diseases: a systematic review. *Gut* **61**, 1619-1635 (2012).

16 Nugent, S. G., Kumar, D., Rampton, D. S. & Evans, D. F. Intestinal luminal pH in inflammatory bowel disease: possible determinants and implications for therapy with aminosalicylates and other drugs. *Gut* **48**, 571-577 (2001).

17 Zhang, S. F. *et al.* An inflammation-targeting hydrogel for local drug delivery in inflammatory bowel disease. *Sci. Transl. Med.* **7**, 300ra128-300ra128 (2015).

18 Kotla, N. G. *et al.* Bioresponsive drug delivery systems in intestinal inflammation: State-of-the-art and future perspectives. *Adv. Drug Deliv. Rev.* **146**, 248-266, doi:10.1016/j.addr.2018.06.021 (2019).

19 Neurath, M. F. Cytokines in inflammatory bowel disease. *Nat. Rev. Immunol.* **14**, 329-342 (2014).

20 Biton, M. *et al.* T helper cell cytokines modulate intestinal stem cell renewal and differentiation. *Cell* **175**, 1307-1320 e1322 (2018).

21 Schwartz, D. M. *et al.* JAK inhibition as a therapeutic strategy for immune and inflammatory diseases. *Nat. Rev. Drug Discov.* **16**, 843-862 (2017).
22 Neurath, M. F. Targeting immune cell circuits and trafficking in inflammatory bowel disease. *Nat. Immunol.* **20**, 970-979 (2019).
23 Ley, K., Rivera-Nieves, J., Sandborn, W. J. & Shattil, S. Integrin-based therapeutics: biological basis, clinical use and new drugs. *Nat. Rev. Drug Discov.* **15**, 173-183 (2016).
24 Mitroulis, I. *et al.* Leukocyte integrins: role in leukocyte recruitment and as therapeutic targets in inflammatory disease. *Pharmacol. Therapeut.* **147**, 123-135 (2015).
25 Mulloy, B., Hogwood, J., Gray, E., Lever, R. & Page, C. P. Pharmacology of heparin and related drugs. *Pharmacol. Rev.* **68**, 76-141 (2016).
26 Ji, Y. *et al.* A heparin derivatives library constructed by chemical modification and enzymatic depolymerization for exploitation of non-anticoagulant functions. *Carbohydr. Polym.* **249**, 116824 (2020).
27 Beurskens, D. M. H. *et al.* The anticoagulant and nonanticoagulant properties of heparin. *Thromb. Haemost.* **120**, 1371-1383 (2020).
28 Wang, P. *et al.* Heparin: an old drug for new clinical applications. *Carbohydr. Polym.* **295**, 119818 (2022).
29 Yan, Y. *et al.* Mucoadhesive nanoparticles-based oral drug delivery systems enhance ameliorative effects of low molecular weight heparin on experimental colitis. *Carbohydr. Polym.* **246**, 116660 (2020).
30 Tyler, C. J. *et al.* Antibody secreting cells are critically dependent on integrin α4β7/MAdCAM-1 for intestinal recruitment and control of the microbiota during chronic colitis. *Mucosal Immunol.* **15**, 109-119 (2022).
31 Diamond, M. S., Alon, R., Parkos, C. A., Quinn, M. T. & Springer, T. A. Heparin is an adhesive ligand for the leukocyte Mac-1(CD11b, CD18). *J. Cell Biol.* **130**, 1473-1482 (1995).
32 Bhattacharyya, A., Chattopadhyay, R., Mitra, S. & Crowe, S. E. Oxidative stress: an essential factor in the pathogenesis of gastrointestinal mucosal diseases. *Physiol. Rev.* **94**, 329-354 (2014).
33 Wilson, D. S. *et al.* Orally delivered thioketal nanoparticles loaded with TNF-α-siRNA target inflammation and inhibit gene expression in the intestines. *Nat. Mater.* **9**, 923-928 (2010).
34 Lee, S., Stubelius, A., Hamelmann, N., Tran, V. & Almutairi, A. Inflammation-responsive drug-conjugated dextran nanoparticles enhance anti-inflammatory drug efficacy. *ACS Appl. Mater. Interfaces* **10**, 40378-40387 (2018).
35 Stubelius, A., Lee, S. & Almutairi, A. The chemistry of boronic acids in nanomaterials for drug delivery. *Acc. Chem. Res.* **52**, 3108-3119 (2019).
36 Nathan, C. & Cunningham-Bussel, A. Beyond oxidative stress: an immunologist's guide to reactive oxygen species. *Nat. Rev. Immunol.* **13**, 349-361 (2013).
37 Sies, H. *et al.* Defining roles of specific reactive oxygen species (ROS) in cell biology and physiology. *Nat. Rev. Mol. Cell Biol.* **23**, 499-515 (2022).
38 Gao, C. *et al.* Treatment of atherosclerosis by macrophage-biomimetic nanoparticles via targeted pharmacotherapy and sequestration of proinflammatory cytokines. *Nat. Commun.* **11**, 2622 (2020).
39 Du, X. *et al.* Polylysine and cysteine functionalized chitosan nanoparticle as an efficient

platform for oral delivery of paclitaxel. *Carbohydr. Polym.* **229**, 115484 (2020).

40 Yen, T. H. & Wright, N. A. The gastrointestinal tract stem cell niche. *Stem Cell Rev. Rep.* **2**, 203-212 (2006).

41 Hindryckx, P., Jairath, V. & D'Haens, G. Acute severe ulcerative colitis: from pathophysiology to clinical management. *Nat. Rev. Gastroenterol. Hepatol.* **13**, 654-664, doi:10.1038/nrgastro.2016.116 (2016).

42 Broaders, K. E., Grandhe, S. & Frechet, J. M. A biocompatible oxidation-triggered carrier polymer with potential in therapeutics. *J. Am. Chem. Soc.* **133**, 756-758 (2011).

43 Wu, J., Zhang, C., Mei, X., Li, Y. & Xing, X. H. Controllable production of low molecular weight heparins by combinations of heparinase I/II/III. *Carbohydr. Polym.* **101**, 484-492 (2014).

44 Xu, J. *et al.* Probiotic-inspired nanomedicine restores intestinal homeostasis in colitis by regulating redox balance, immune responses, and the gut microbiome. *Adv. Mater.* **35**, e2207890 (2023).

Data availability

All data supporting the results in this study are available within the paper and its Supplementary Information. Additional processed data are available from the corresponding authors on request.

Acknowledgements

This work was supported by grants from the Key Research and Development Program of the Ministry of Science and Technology (2023YFA0914300), Shenzhen Medical Research Fund (SMRF, B2302009), National Natural Science Foundation of China (22161142014), State Administration for Market Regulation (SAMR) Technical Guarantee Project (2023YJ22) and Hebei Administration for Market Regulation Technology Project (2024ZD02).

Author contributions

XH. X. Y. W. and CY. Z. oversaw all research. L. H., B. X., Y. W., CY. Z. and XH. X. designed the research strategy. L. H. synthesized materials and fabricated nanotherapy. L. H., LQ. H., W. H., QX. Z., ZY. S., and HY. T. performed experiments. L. H. and Y. W. analyzed experiments. L. H., Y. W., CY. Z. and XH. X. prepared for the manuscript. All authors approved the manuscript.

Competing interests

XH. X., L. H. and Y. W. are inventors on related patents filed by Tsinghua University describing the materials and nanotherapy reported in this study. The other authors declare no competing interests.

Supplementary Information

"Hitting Two Birds with One Stone" Design of Intestinal Integrin-Targeting and Redox Homeostasis-Regulating Oral Nanotherapy for Ulcerative Colitis

Contents

Supplementary Scheme 1 | Synthesis of OsEPL.
Supplementary Fig. 1 | Schematic illustration of the preparation and degradation of OsEPL.
Supplementary Fig. 2 | ^{1}H-NMR spectrum of imidazoyl carbamate (Compound 1) in DMSO-d_6.
Supplementary Fig. 3 | ^{1}H-NMR spectrum of EPL in DMSO-d_6.
Supplementary Fig. 4 | ^{1}H-NMR spectrum of OsEPL in DMSO-d_6.
Supplementary Fig. 5 | Physicochemical properties of OsEPL.
Supplementary Fig. 6 | Molecular weight distribution of UFH and LMWH determined by GPC.
Supplementary Fig. 7 | Stability of OPNs and OPNs@LMWH.
Supplementary Fig. 8 | OPNs@LMWH are internalized by M1 macrophages.
Supplementary Fig. 9 | Quantitative analysis of FA fluorescence intensity of internalized nanoparticles
Supplementary Fig. 10 | High level of CD11b in the colonic submucosal layer of colitis mice.
Supplementary Fig. 11 | OPNs@LMWH accumulates in inflamed colon infiltrated by inflammatory cells.
Supplementary Fig. 12 | Cytotoxicity testing determined by CCK-8.
Supplementary Fig. 13 | Concentration-dependent intracellular ROS-scavenging behavior.
Supplementary Fig. 14 | LMWH presents little anti-ROS property.
Supplementary Fig. 15 | Concentration of Free LMWH determined by Azure A.
Supplementary Fig. 16 | Safety profiles of OPNs@LMWH (body weight).
Supplementary Fig. 17 | Safety profiles of OPNs@LMWH (major organs).
Supplementary Fig. 18 | Safety profiles of OPNs@LMWH (blood hematology).

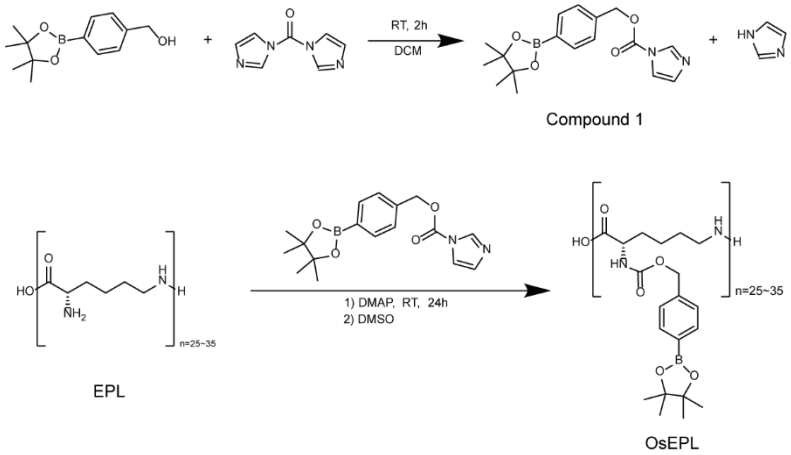

742
743 **Supplementary Scheme 1 | Synthesis of OsEPL.**
744
745

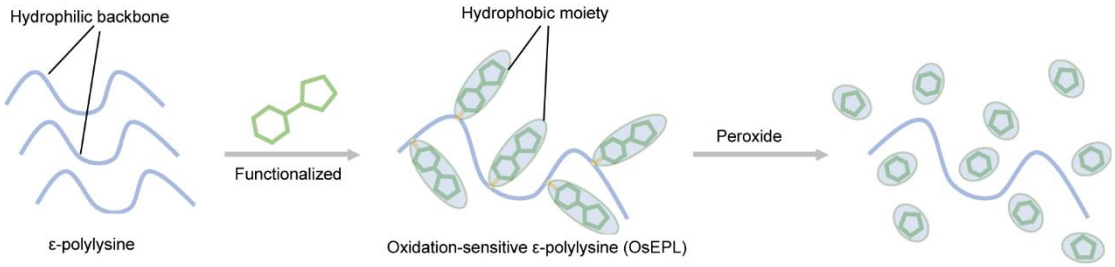

746
747 **Supplementary Fig. 1 | Schematic illustration of the preparation and degradation of**
748 **OsEPL.**
749

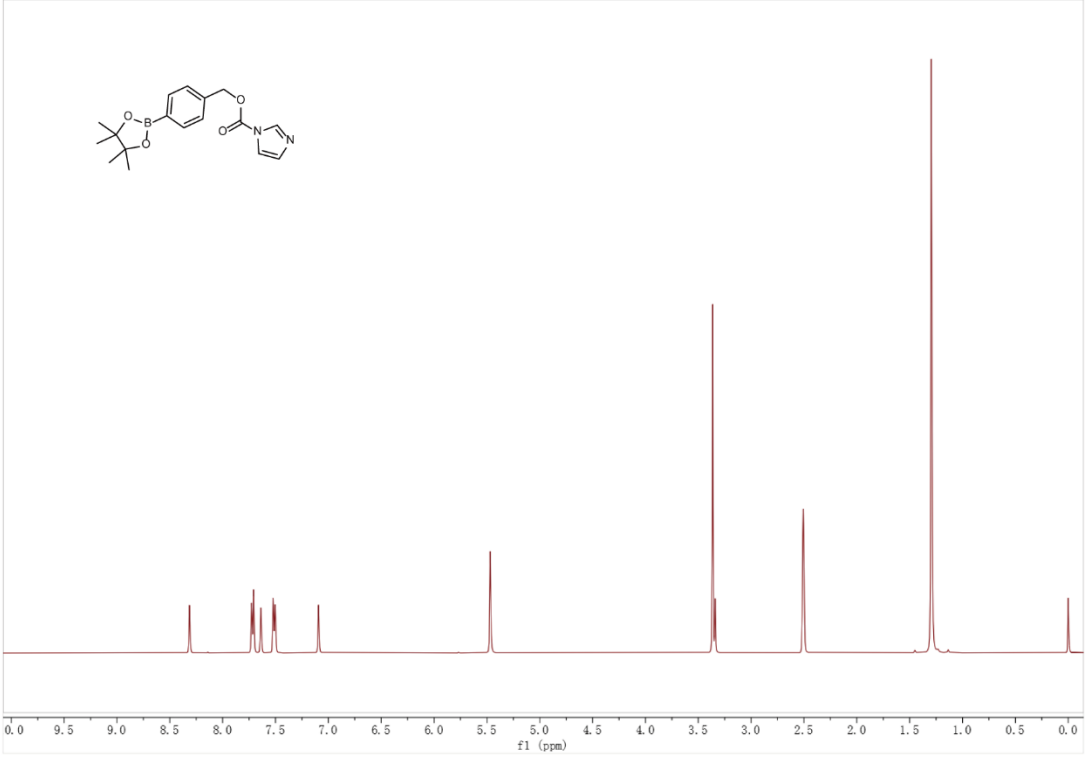

Supplementary Fig. 2 | ^{1}H-NMR spectrum of imidazoyl carbamate (Compound 1) in DMSO-d_6.

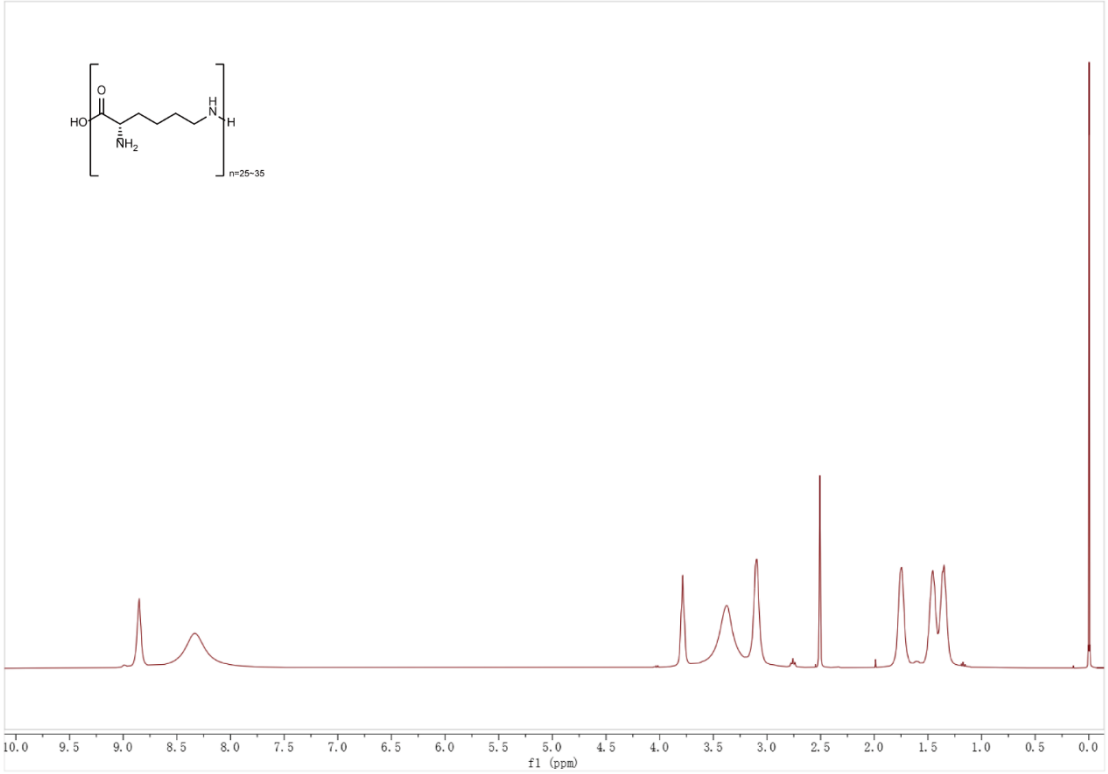

Supplementary Fig. 3 | ^{1}H-NMR spectrum of EPL in DMSO-d_6.

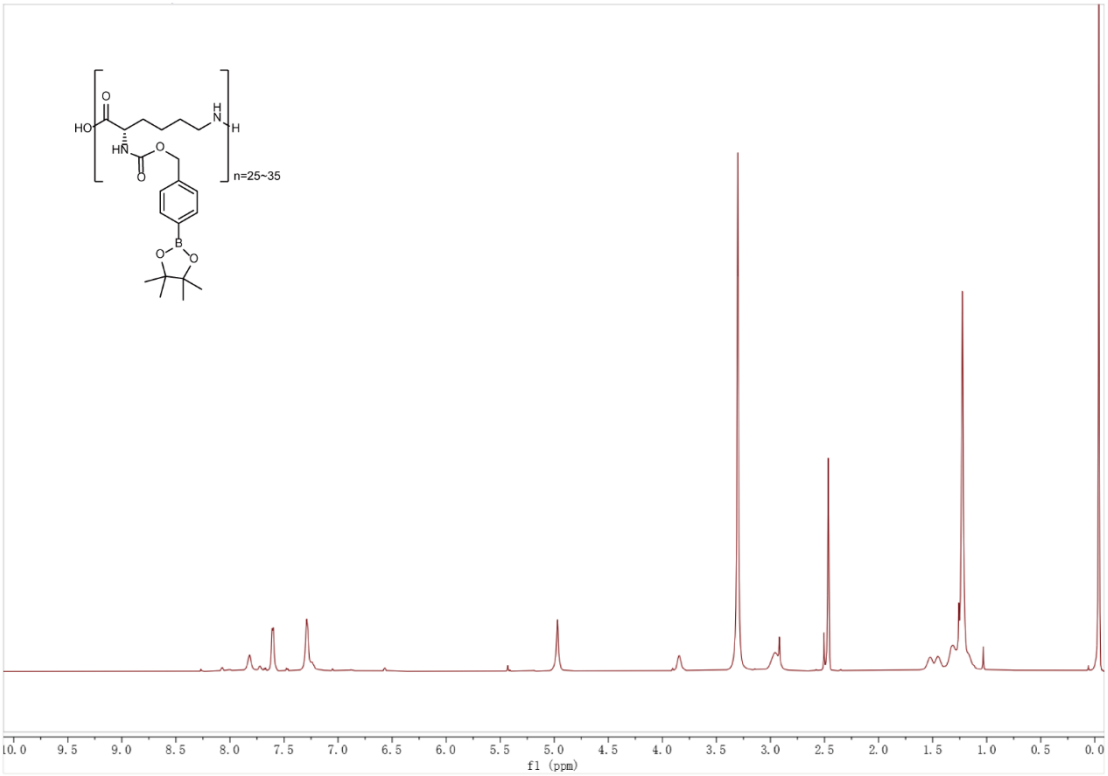

Supplementary Fig. 4 | ^{1}H-NMR spectrum of OsEPL in DMSO-d$_6$.

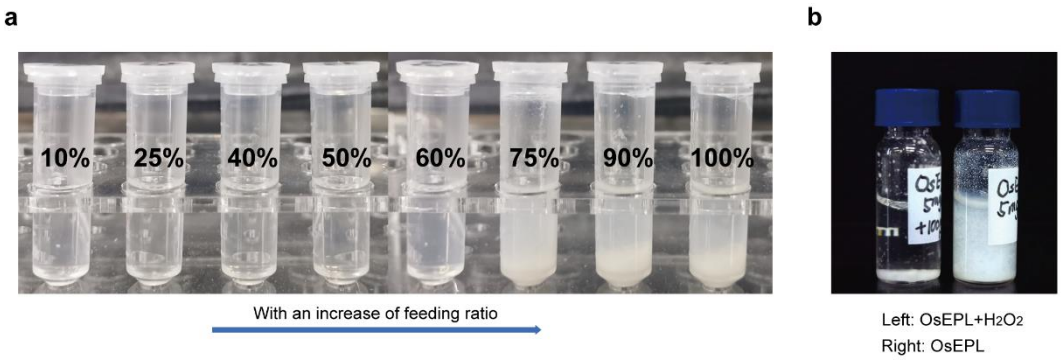

Supplementary Fig. 5 | Physicochemical properties of OsEPL. a, A series of OsEPL with different feeding ratios of phenylboronic acid pinacol ester and amino presented varying amphiphilicity. **b,** OsEPL was incubated with 100 mM H_2O_2 for one hour.

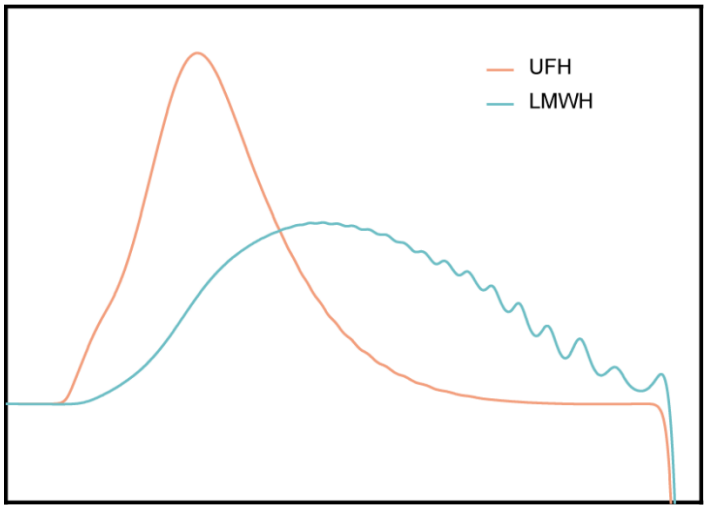

Supplementary Fig. 6 | Molecular weight distribution of UFH and LMWH determined by GPC.

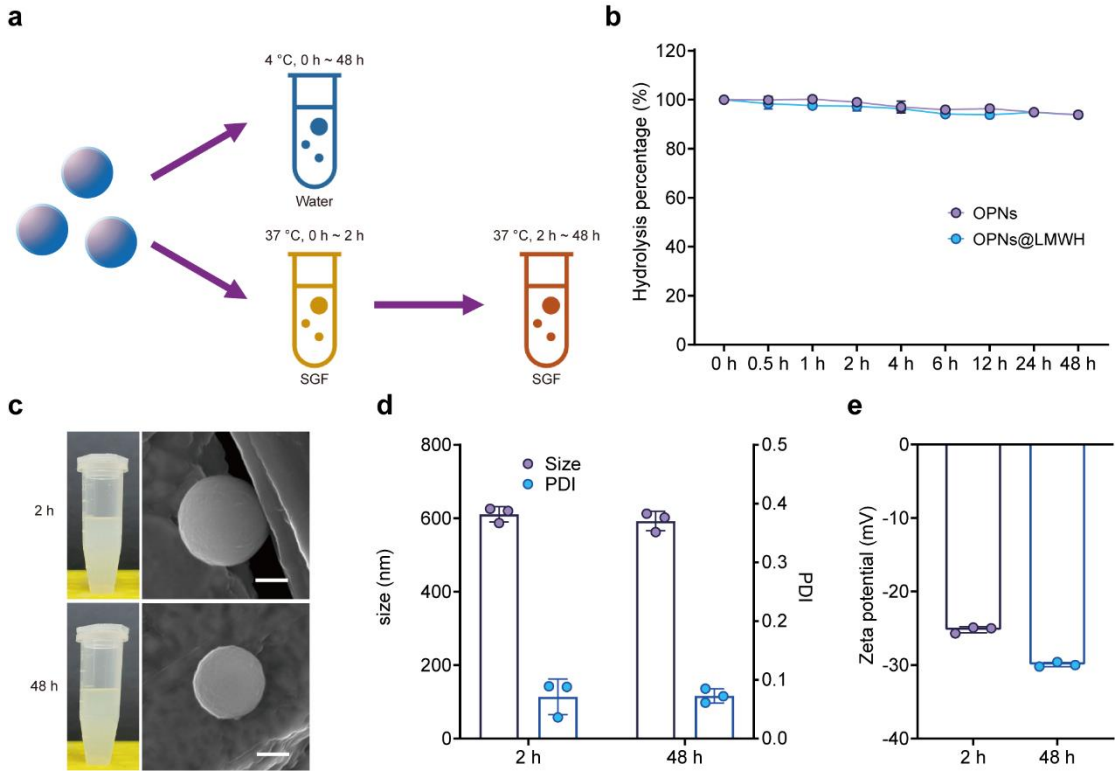

Supplementary Fig. 7 | Stability of OPNs and OPNs@LMWH. a, OPNs and OPNs@LMWH were incubated under storage condition (deionized water, 4 °C) or simulated digestion process (SGF, 2 h, 37 °C and SIF, 46 h, 37 °C). **b,** The hydrolysis ratio of nanoparticles under storage conditions. **c-e,** Representative SEM image (**c**), particle size (**d**) and zeta potential (**e**) of OPNs@LMWH incubated under simulated digestion process. of Shown are quantitative analysis from n= 3 biologically independent samples. Data represent mean ±SD.

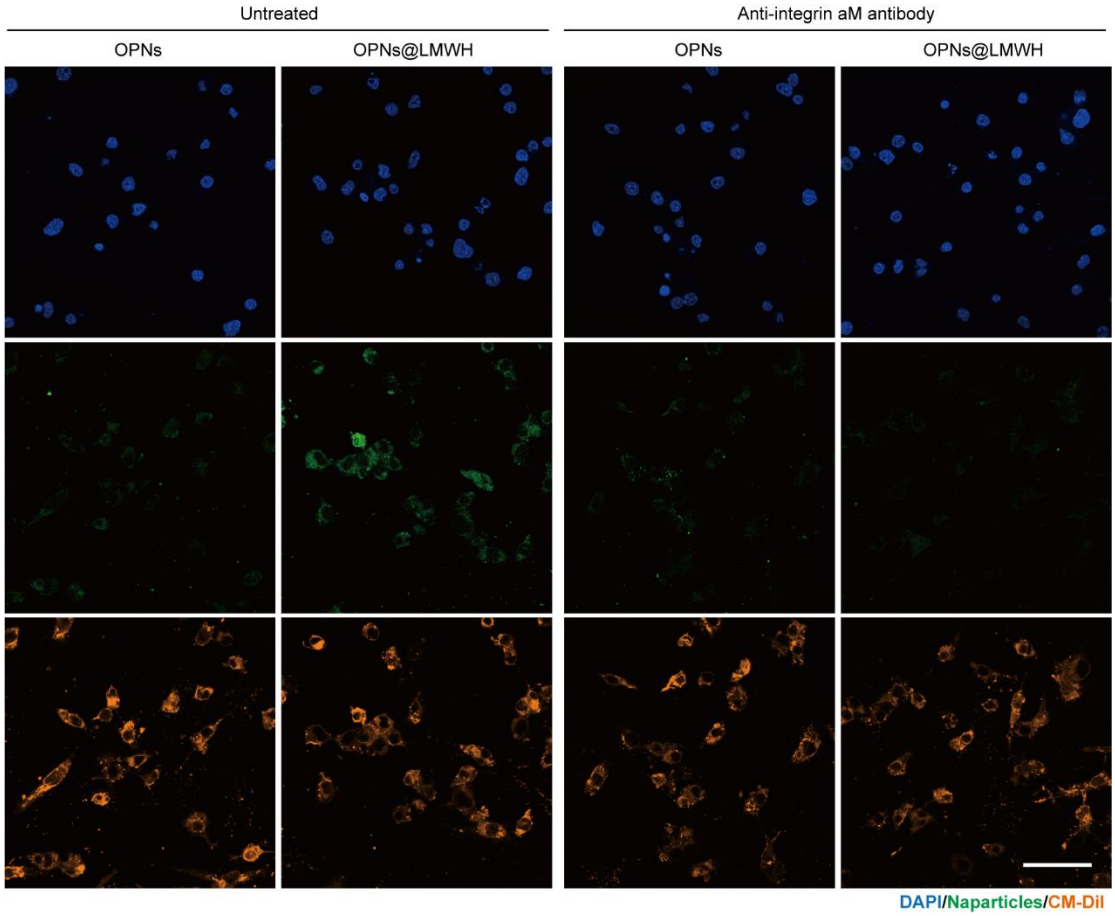

Supplementary Fig. 8 | OPNs@LMWH are taken up by integrin αM+ cells. Activated RAW264.7 cells were incubated with FA-OPNs or FA-OPNs@LMWH and pretreated with or without anti-integrin αM antibody, visualized by CLSM. Scale bar, 50 μm. Shown are representative images of n=6 biologically independent samples.

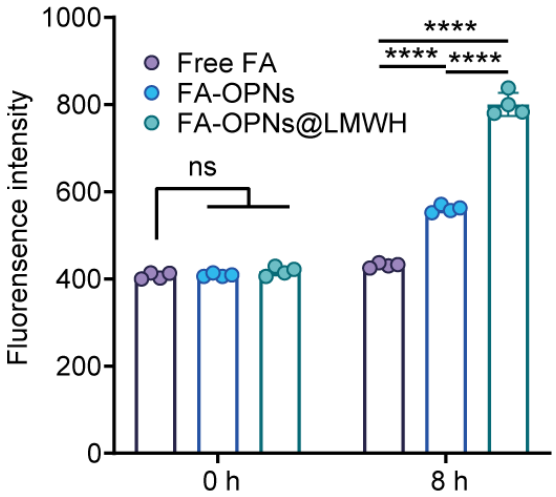

Supplementary Fig. 9 | Quantitative analysis of FA fluorescence intensity of internalized nanoparticles. FA fluorescence intensity determined by flow cytometry confirmed that free FA were not allowed to entrance. Shown are quantitative analysis from n= 4 biologically

independent samples. Data represent mean ±SD. * $p < 0.05$, ** $p < 0.01$, *** $p < 0.001$, **** $p < 0.0001$ and ns $p > 0.05$, analyzed by two-way ANOVA multiple comparisons test.

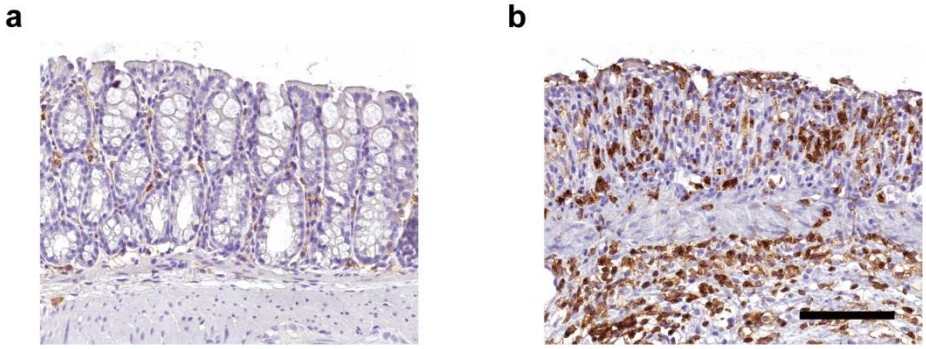

Supplementary Fig. 10 | High level of CD11b in the colonic submucosal layer of colitis mice. Representative images of immunohistochemical staining for CD11b in health (**a**) or colitis (**b**) mice. Scale bar, 100 μm. Shown are representative images from n= 3 biologically independent samples.

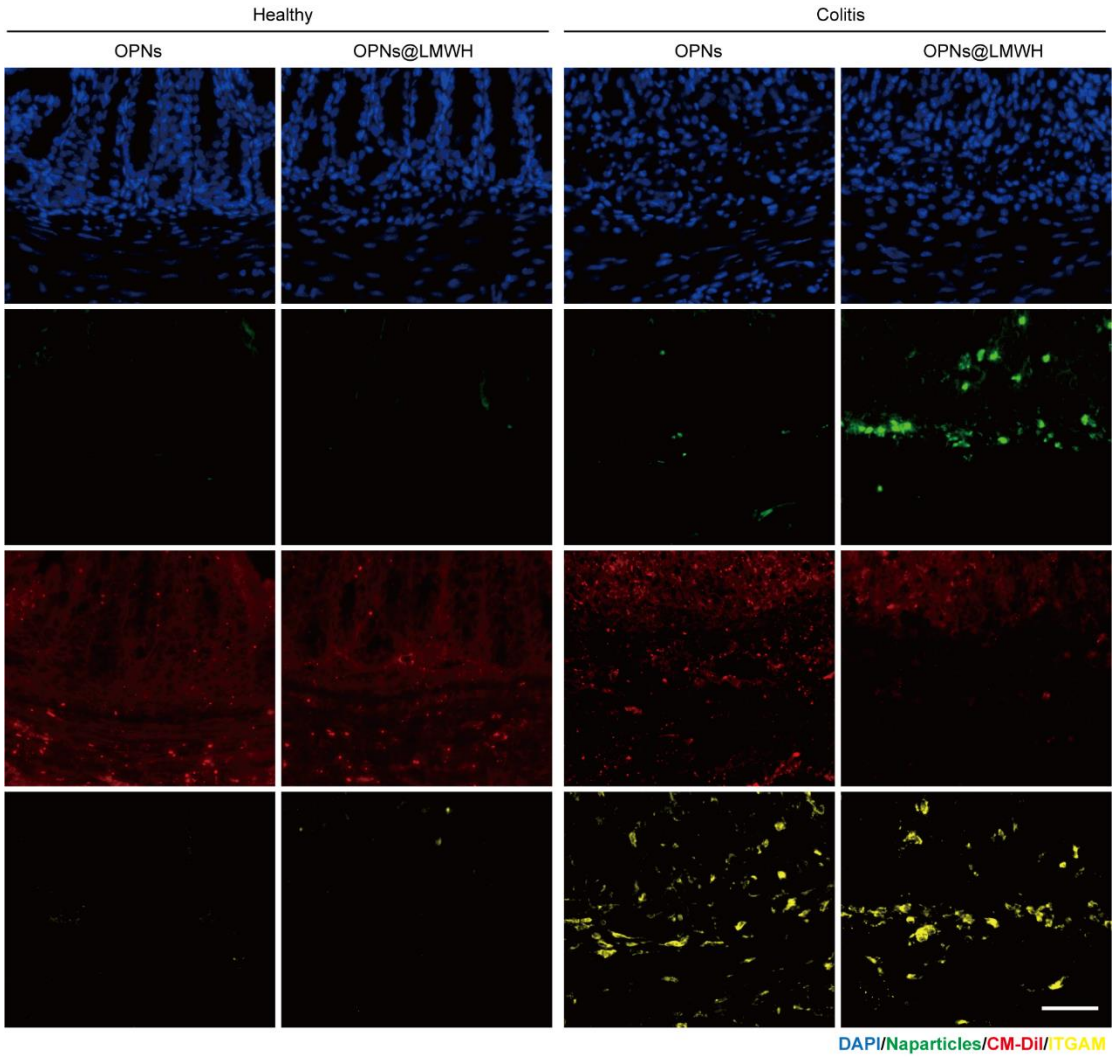

Supplementary Fig.11 | OPNs@LMWH accumulates in inflamed colon infiltrated by inflammatory cells. Healthy or colitis mice were orally administrated with FA-OPNs or FA-OPNs@LMWH, and colon tissues were collected after 24 h and stained with DAPI, CM-Dil and ITGAM, visualized by CLSM. Scale bar, 50 μm. Shown are representative images of n=3 animals.

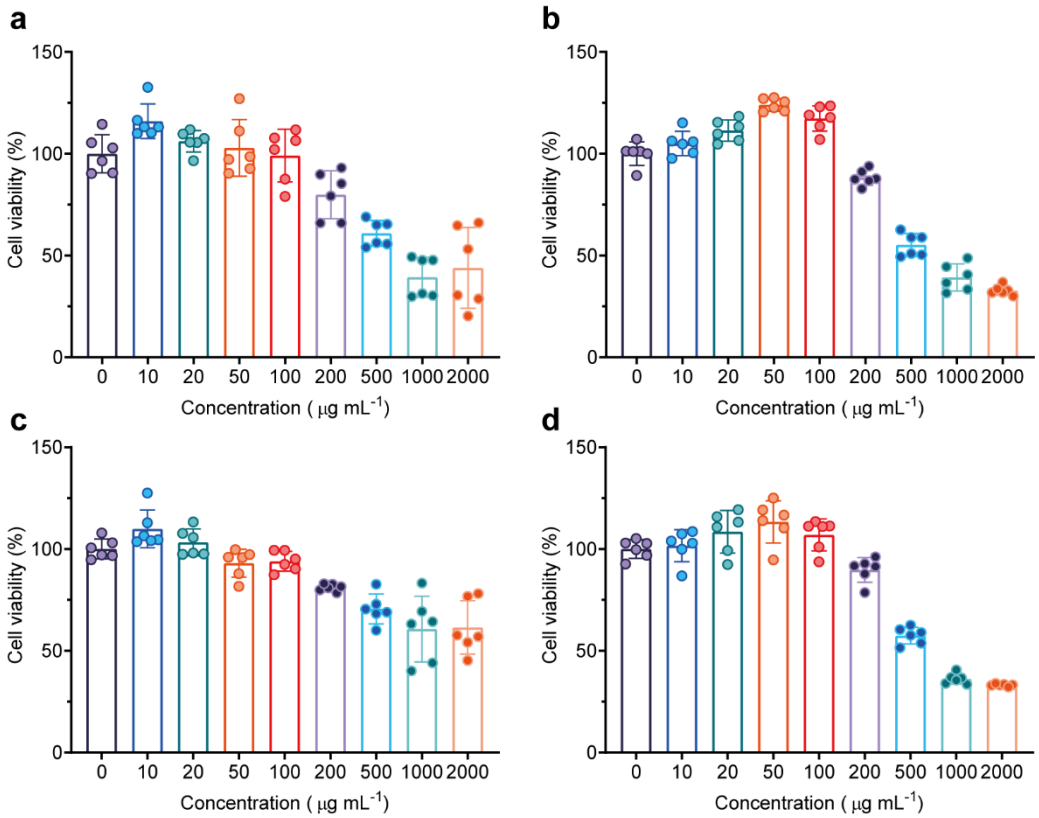

Supplementary Fig. 12 | Cytotoxicity testing determined by CCK-8. a, b, Cell viability of OPNs incubated with RAW264.7 cells (**a**) and NCM460 cells (**b**) for 24 h. **c, d,** Cell viability of OPNs@LMWH incubated with RAW264.7 cells (**c**) and NCM460 cells (**d**) for 24 h. Shown are quantitative analysis from n= 6 biologically independent samples (**a-d**). Data represent mean ±SD.

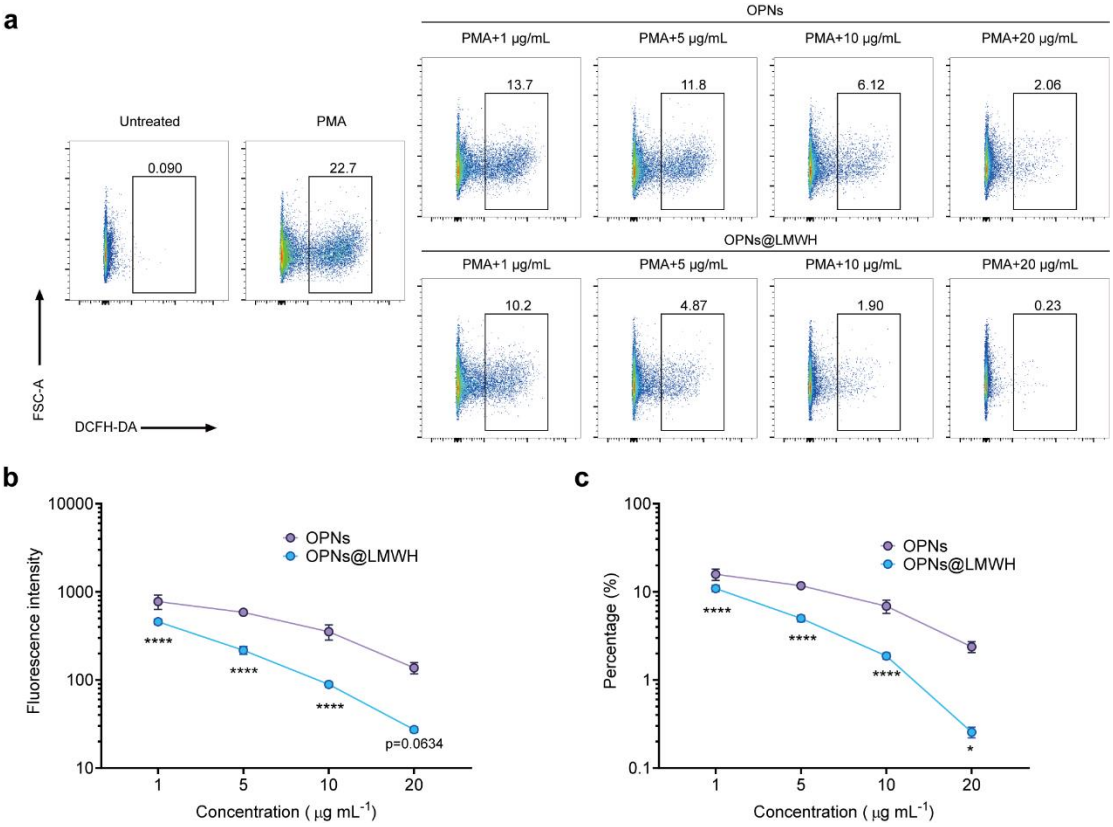

Supplementary Fig. 13 | Concentration-dependent intracellular ROS-scavenging behavior. a, RAW264.7 cells were stimulated with PMA and treated with OPNs or OPNs@LMWH with different concentration. **b, c,** Fluorescence intensity (**b**) and percentage of ROS-positive cell (**c**) were calculated. Shown are representative gating strategy or quantitative analysis from n= 4 biologically independent samples (**a-c**). Data represent mean ±SD. * $p < 0.05$, ** $p < 0.01$, *** $p < 0.001$, **** $p < 0.0001$ and ns $p > 0.05$, analyzed by two-way ANOVA multiple comparisons test (**b, c**).

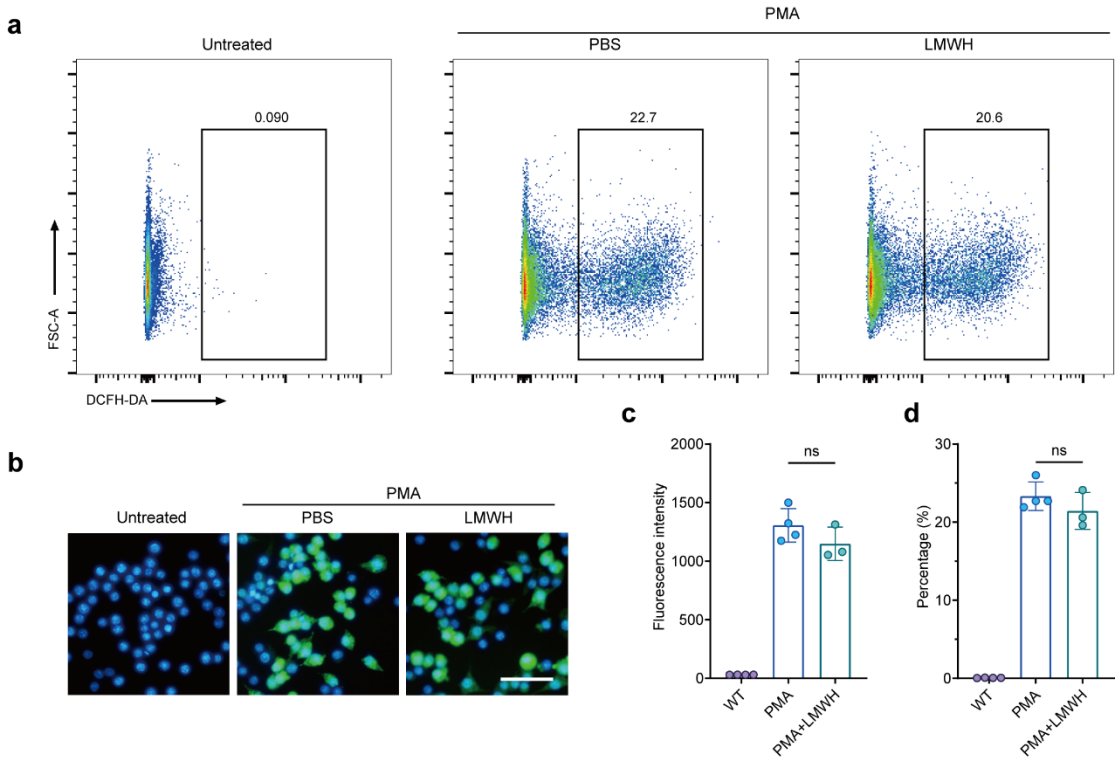

Supplementary Fig. 14 | LMWH presents little anti-ROS property. a, b, RAW264.7 cells were stimulated with PMA and treated with LMWH (20 μg/mL). **c, d,** Fluorescence intensity (**c**) and percentage of ROS-positive cell (**d**) were calculated. Shown are representative gating strategy, images or quantitative analysis from n= 3 or 4 biologically independent samples (**a-d**). Data represent mean ±SD. * $p < 0.05$, ** $p < 0.01$, *** $p < 0.001$, **** $p < 0.0001$ and ns $p > 0.05$, analyzed by unpaired t test (**c, d**).

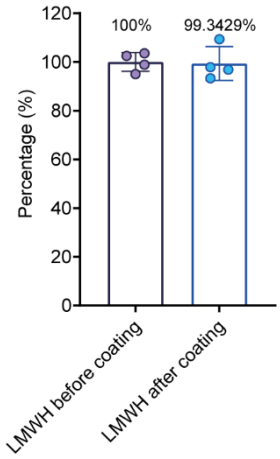

Supplementary Fig. 15 | Concentration of Free LMWH determined by Azure A. Free LMWH in supernatant before or after coating were detected and indicated low mass proportion of LMWH in OPNs@LMWH. Shown are quantitative analysis from n= 4 biologically independent samples.

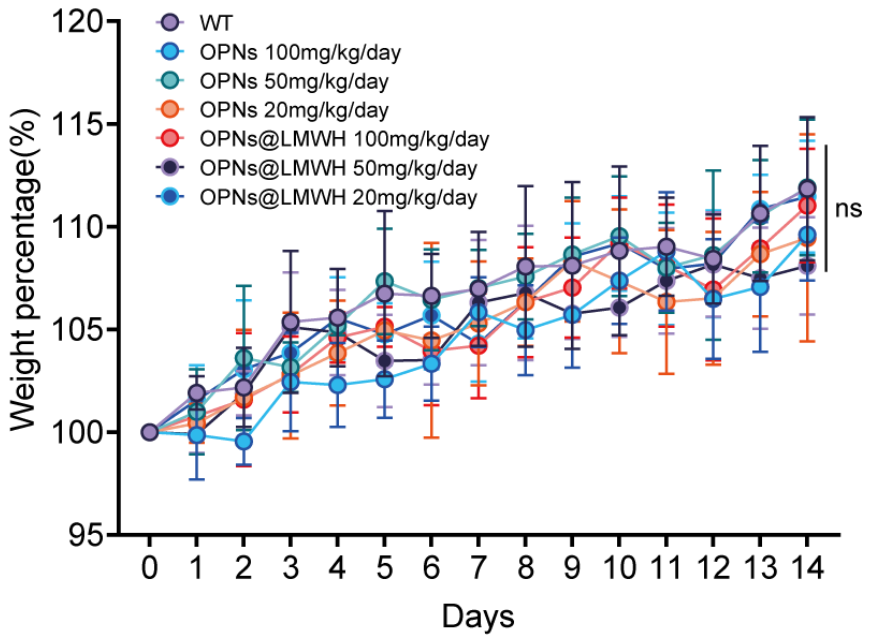

Supplementary Fig. 16 | Safety profiles of OPNs@LMWH (body weight). Mice were orally administrated with different dose of nanoparticles for 14 days. Daily body weight changes were recorded. Shown are quantitative analysis from n=6 animals. Data represent mean ±SD. * $p < 0.05$, ** $p < 0.01$, *** $p < 0.001$, **** $p < 0.0001$ and ns $p > 0.05$, analyzed by two-way ANOVA multiple comparisons test (**b, c**).

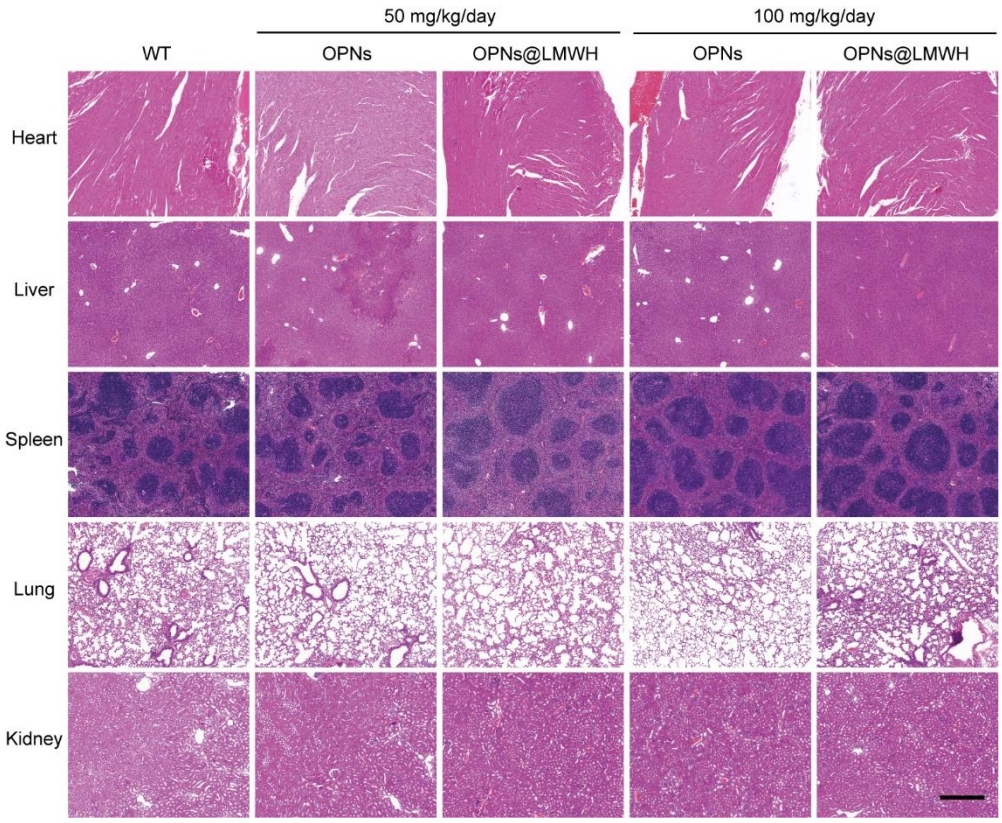

Supplementary Fig. 17 | Safety profiles of OPNs@LMWH (major organs). Mice were sacrificed on day 14. Major organ (heart, liver, kidney, lung, spleen, and colon) sections were stained with hematoxylin and eosin. Shown are representative images from n= 3 animals.

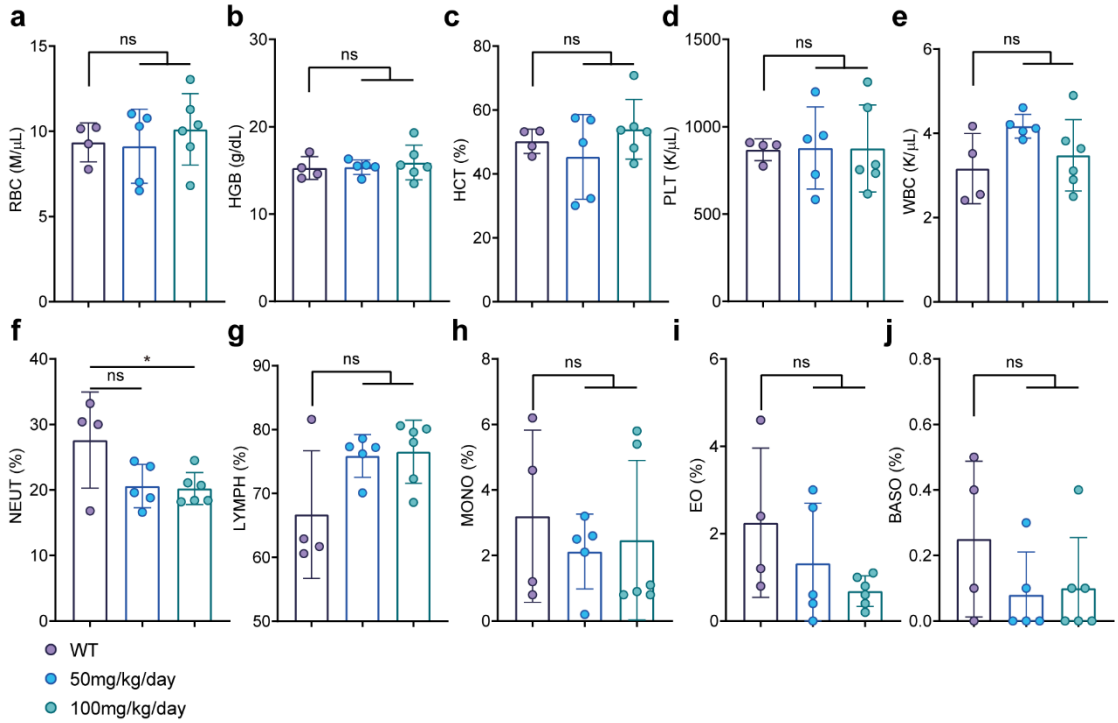

Supplementary Fig. 18 | Safety profiles of OPNs@LMWH (blood hematology). Mice were sacrificed on day 14. The blood samples were collected and analyzed by using blood hematology, including red blood cell count (RBC) (**a**), hemoglobin (HGB) (**b**), hematocrit (HCT) (**c**), platelet (PLT) (**d**), white blood cell count (WBC) (**e**), neutrophil (NEUT) (**f**), lymphocyte (LYMPH) (**g**), monocyte (MONO) (**h**), eosinophil (EO) (**i**) and basophil (BASO) (**j**). Shown are quantitative analysis from n= 4-6 animals. Data represent mean ±SD. * $p < 0.05$, ** $p < 0.01$, *** $p < 0.001$, **** $p < 0.0001$ and ns $p > 0.05$, analyzed by ordinary one-way ANOVA multiple comparisons test.